2020

EFFICIENT ENHANCEMENT OF MICRO-NUCLEATION RATES IN FLOW-BOILING - BY CONCURRENT MICRO-STRUCTURING OF THE BOILING-SURFACE AND ITS JUDICIOUS ENERGIZATION BY PIEZOELECTRIC-TRANSDUCER INDUCED ACOUSTIC VIBRATIONS.

ATHARVA RAHANE
Michigan Technological University, arahane@mtu.edu

EFFICIENT ENHANCEMENT OF MICRO-NUCLEATION RATES IN FLOW-BOILING - BY CONCURRENT MICRO-STRUCTURING OF THE BOILING-SURFACE AND ITS JUDICIOUS ENERGIZATION BY PIEZOELECTRIC-TRANSDUCER INDUCED ACOUSTIC VIBRATIONS.

By

Atharva Rahane

A REPORT

Submitted in partial fulfillment of the requirements for the degree of

MASTER OF SCIENCE

In Mechanical Engineering

MICHIGAN TECHNOLOGICAL UNIVERSITY

2020

This report has been approved in partial fulfillment of the requirements for the Degree of MASTER OF SCIENCE in Mechanical Engineering.

Department of Mechanical Engineering-Engineering Mechanics

Thesis Advisor: *Dr. Amitabh Narain*

Committee Member: *Dr. Sunil Mehendale*

Committee Member: *Dr. Kazuya Tajiri*

Department Chair: *Dr. William W. Predebon*

Table of Contents

List of figures iv

List of tables vi

Preface vii

Acknowledgments viii

Definitions ix

List of abbreviations xii

Abstract xiii

1 Introduction 1

1.1 Motivation 2

2 Experimental Setup and Description 9

3 Results 15

4 Discussions 32

4.1 Micro Nucleating Bubble Diameter 32

4.2 Thermal Circuit and Mesh Top Temperatures 34

4.3 Contact Angle 36

4.4 Other Related Insights/Discussions of the Underlying Flow-Physics 37

5 Future Scope and Directions 41

6 Conclusions 42

7 Reference List 43

List of figures

Figure 1.1. Typical flow-boiling regimes and regimes of interest for proposed heatsink operations. 2

Figure 1.2. Often invisible micro-nucleation in the annular regime-B of (Figure 1.1) above can be inferred (or made visible by suitable magnifications within the highlighted box) to conclude their presence, as shown. 3

Figure 1.3. Presence of invisible μm- scale nucleation rates (bubble diameters less than 10 μm) for observed liquid thickness $\Delta \cong O$ (100-300 μm) leads to an equivalent liquid thickness ΔF that is much less and is a result of micro-scale nucleation rates. 4

Figure 1.4. The figure shows enhanced HTC across equivalent liquid thickness ΔF. However, liquid flow mobility continues to be superior – as in Figure 1.3. 4

Figure 1.5. Nucleate/bubbly regime of operations with several new micron-sized bubbles (●) of diameter D_b induced by the proposed technology. 5

Figure 1.6. Mechanisms and contact-line physics for nucleate boiling ebullition cycle. The figure also highlights the significant heat-flux impact of advancing/receding dynamics of micro-layers and the role of oscillatory contact-line interfacial shear (whether induced entirely naturally by heat – or supplemented by mechanical actuation)....6

Figure 1.7. Bubble formation over the boiling surface at any instant time t. 7

Figure 1.8. Time evolution of a bubble for a respective fixed location P – see (1.7) – on the boiling surface. 7

Figure 1.9. Cross-sectional view of a small portion of the boiling surface is taken from the test section in Figure 2.1, shows a mesh with piezo actuations. Only the last pillar (formed by stack of the copper mesh) in the above figure is shown displaced but all of them (entire mesh) vibrate at a resonant frequency. There are green nucleating vapor bubbles in the tiny crevices of the mesh which rise and are fed to a relatively larger bubble on the distal tip. The oscillating motion of the tip induce hydrodynamic forces that results in the dislodging of bubble at a much smaller diameter....8

Figure 2.1. Test section....12

Figure 2.2. Standard arrangements of the experimental flow-loop. 13

Figure 2.3. Axial cross-sectional view....13

Figure 2.4. Lateral cross-sectional view 14

Figure 2.5. Experimental setup at present.....14

Figure 3.1. Heater block and test section assembly. 17

Figure 3.2. Resistance to the heat flux where Rboiling represents the resistance in different conditions of boiling (no mesh, with mesh and mesh + piezo enhanced boiling). The effective resistance offered by the mesh is Rmesh and Rboiling plate is the resistance due to the copper boiling plate below the mesh. 24

Figure 3.3. Thermal circuit. 25

Figure 3.4. Heat Transfer Coefficient (heff) vs Heat Flux Experimental data and Corrected K-M plots for three different experimental scenarios. 29

Figure 3.5. Heat Transfer Coefficient ($h_{boiling-model}$) vs Heat Flux Corrected K-M plots for three different experimental scenarios.....29

Figure 3.6. Heat Transfer Coefficient (heff) vs Heat Flux Corrected K-M Blueprint.....30

Figure 3.7. Heat Transfer Coefficient ($h_{boiling-model}$) vs Heat Flux Corrected K-M Blueprint. 30

Figure 3.8. The test-section pressure's ($P_{test-sec}$) time response to increased micro-nucleation rates. 31

Figure 4.1. Wenzel filling of the mesh with tiny white spots as potential nucleation sites on the mesh. 37

List of tables

Table 1. Results from test runs for representative no-piezo actuation and plain copper boiling cases. The representative constant density of the liquid phase is denoted by ρ_L.....18

Table 2. Results from test runs for representative no-piezo actuation and meshed boiling surface cases. The representative constant density of the liquid phase is denoted by ρ_L.....18

Table 3. Results from flow-boiling test runs for representative "meshed boiling-surfaces with piezos' actuation." The representative constant density of the liquid phase is denoted by ρ_L. The controller settings are given in the second column from the left. Number of pulses denote $\Delta ton \cdot fp$ values.....20

Table 4. Results from flow-boiling test runs for representative "meshed boiling-surfaces with piezos' actuation." The representative constant density of the liquid phase is denoted by ρ_L. Totally different controller settings are associated with totally different hardware (copper block and meshed surfaces). 20

Preface

This report is an extension of the work and materials used in [1]. Sections dealing with the abstract, section-1, section-2, experimental data in section-3, and section 4.1 are more or less directly taken from [1,4] and its supplementary documents

The purpose of doing this is to improve the readability of the report and to better highlight my independent contributions. The new modelling and results described in section 3 and sections 4-5 (minus section 4.1) are new works done by me (under the guidance of Dr. Narain and his team).

Acknowledgments

The entirety of this report has been carried out at Michigan Technological University during the years 2019-2020, under the guidance of Professor Dr. Amitabh Narain.

I would like to thank my advisor, Dr. Amitabh Narain, for giving me the opportunity to work on this project and for the constant encouragement. My heartiest thanks are due to Divya Pandya, a MEEM doctoral student being advised by Dr. Narain, for the support and guidance provided throughout this report.

I would also like to take the opportunity to thank my parents, family and friends for their constant emotional support and encouragement.

Definitions

$\dot{M}_{L\text{-}in}$ = Mass flow rate of liquid HFE 7100 entering the test section

$\dot{M}_{V\text{-}out}$ = Mass flow rate of HFE 7100 vapor exiting the test section

$\dot{M}_{L\text{-}out}$ = Mass flow rate of liquid HFE 7100 exiting the test section

T_{mt-avg} = Average mesh top temperature

$T_{mt-local}$ = Temperature measured at the top of the mesh by RTD adjacent to the copper tip

T_{tbp} = Average temperature at the top of the boiling plate

T_{bbp} = Average temperature at the bottom of the boiling plate

T_{sat} = Saturation temperature of HFE7100 corresponding to the approximate unit average pressure inside the test section

$P_{test\text{-}sec}$ = Pressure measured by the pressure transducer inside the test section

ΔT_{rep} = Difference between temperatures T_{tbp} and T_{sat} represents a driving temperature responsible for heat flow through the heat-sink mounted on a heating device

T_{HB1} = Heater block temperature at location (1) in Figure 2.2. Locations (1, 2, & 3) are on the same horizontal surface.

T_{HB2} = Heater block temperature at location (2) in Figure 2.2.

T_{HB3} = Heater block temperature at location (3) in Figure 2.2.

T_{HB4} = Heater block temperature at location (4) in Figure 2.2.

$\overline{T}_{HB2}$= Average of temperatures measured at locations (1, 2, & 3)

d_{42} = Vertical distance between locations (4) and (2) approximately 1.13 mm in Figure 2.4

A_{bs} = Boiling surface area

L_{bp} = Boiling plate thickness

L_{mesh} = Mesh thickness

k_{cu} = Thermal conductivity of copper (heater block)

q''_w = Estimated heat flux (W/cm^2) over the boiling-surface (of area A_{bs} = 2 cm^2). Heat (in W) entering the test section – approximately $q''_w \cdot$.

f_M = The modulating frequency of the square wave imposed by the Piezos' controller.

Δ = Film thickness

Δ_F = Effective fluid thickness

S_x, S_y = Oscillatory in plane shear stresses

D_b^*= Bubble departure diameter

$f_e(D_b^*)$ = Bubble departure frequency which is a function of bubble departure diameter

$n''_{av}(D^*_b)$ = Nucleation site density

List of abbreviations

HTC	Heat Transfer Coefficient
ONB	Onset of Nucleate Boiling
Piezo	Piezoelectric Transducers

Abstract

The report describes the science and technology backgrounds and uses for the technology breakthrough reported for enhanced flow-boiling based cooling of high-power density electronics (chips, memory etc.). A controlled but explosive growth in micro-scale nucleation rates during flow-boiling of HFE-7100 (electronics and environment friendly liquid from 3M, Inc) is enabled by the uses of inexpensive meshed-copper for micro-structuring of the boiling surface and a pair of Piezoelectric-transducers for active imposition of suitable acoustic vibrations. The pair of piezo transducers mounted just outside the mini-channel impose "in plane" acoustic vibrations of controllable amplitudes and frequencies, and they are used to induce phenomena which make flow-boiling highly efficient. Superposition of such active resonant acoustics towards beneficial actuation of the bubbles' ebullition cycles, where mesh-tips' minuscule structural vibrations play key roles, are an important part of the enabling science and technology. Even preliminary results show, relative to currently popular water-based Direct Contact Liquid Cooling (DCLC) or Direct to Chip (D^2C) liquid cooling approaches, heat transfer efficiency goes up by 700%, driving temperature difference goes down by 80-90%, maximum allowed average heat-flux goes up from about 35 W/cm^2 to more than 70 – 100 W/cm^2, and boiling surface temperatures can be adjusted in the range of 50 - 65^{0}C (as needed) relative to the maximum allowed chip junction temperature of 80 - 85^{0}C (or less).

1 Introduction

The science-based efficient high-heat-flux (> 70 - 200 W/cm^2) and low-pressure-drop flow-boiling solution proposed here builds on vigorously researched related efforts of the past two decades or so. Investigations involving micrometer- to millimeter-scale channels, high-heat-flux heating rates, and traditional operations (i.e. all liquid at the inlet to all vapor at the exit) have thus far yielded inefficient and unacceptable performances. Such as lowered heat transfer coefficient (HTC) values leading to, increased driving temperature differences for a given heat-flux, increased pressure-drops, or accompanying instabilities at single channel, multi-channel, and system levels. These are largely because high heat flux impositions necessarily require large liquid mass fluxes (near saturation temperatures) at the inlet and they accompany large magnified vapor volume fluxes at the exit – about 500 – 1000 times the incoming liquid volume fluxes. Traditional operations involving micro-milli diameter short (about 1- 5 cm long) ducts, complete vaporization of the inlet mass-flux, and a single exit (often narrow) exacerbate the problems. To address this situation, and selectively building on insights gained from earlier approaches, micro-structured boiling surface is used in conjunction with thin piezoelectric transducers (mounted outside the boiling channels) to induce resonant "in-plane" vibrations (with minimal energy input) to achieve significantly high cooling rates through improved HTC and low pressure-drops. This improvement in cooling rates result from controlled but explosive growth in micro-nucleation rates achieved by imposition of oscillatory shear plane motions of the more rigid boiling-surface relative to its immediate fluid-filled neighborhood. Also, partial boiling, with constrained exit quality ($x < 0.6$) and special

arrangements that deploy two exit-ports, and flow controls for the two tubes' flows downstream of the two exits, together provide the capability of addressing stability issues while keeping pressure drops low.

1.1 Motivation

Results from steady and steady-in-the-mean shear driven annular flow-boiling experiments presented elsewhere [2-6] lead to a following key conclusion that invisible (below resolution of available sensing capability of the instrument used) micron-scale nucleating bubbles and their nucleation rates (from inception to growth to departure back to inception again) play a very significant role in affecting and enhancing heat-transfer coefficient (HTC) values. HTC represents a form of heat-transfer efficiency whose high values keep the temperature difference low between the cooling-surface temperature and a reference temperature for the coolant flow. The so called "convective" annular regime of flow boiling with thin liquid film (100 – 400 mm) is shown as regime-B in Figure 1.

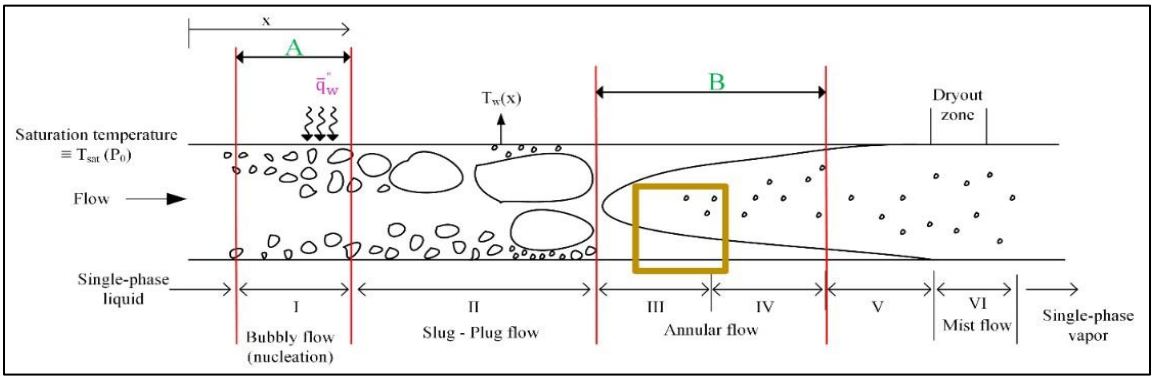

Figure 1.1. Typical flow-boiling regimes and regimes of interest for proposed heatsink operations.

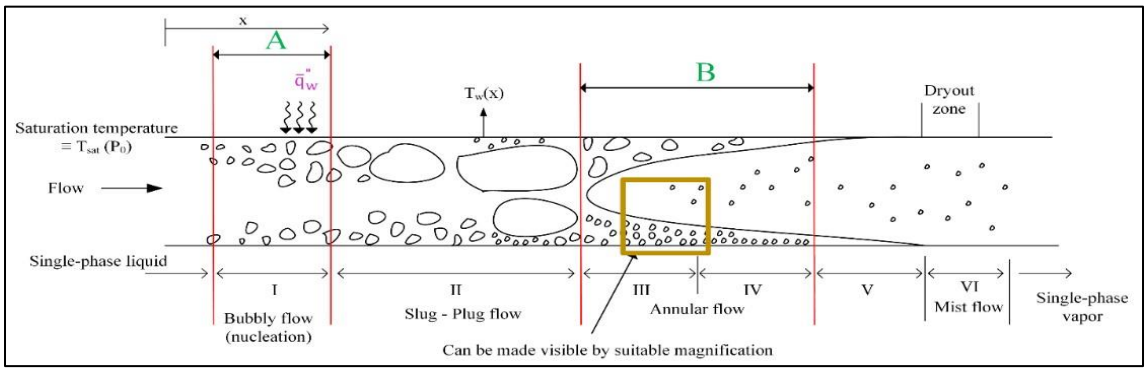

Figure 1.2. Often invisible micro-nucleation in the annular regime-B of (Figure 1.1) above can be inferred (or made visible by suitable magnifications within the highlighted box) to conclude their presence, as shown.

The experiments done in the annular regimes ([2-6] conclusively establish that, typically 80-90% of the measured/estimated total HTC values come from micron-sized nucleating bubbles. Current understanding of bubble's ebullition mechanisms ([7-12]) support the fact that this increase in HTC values come from an effective decrease in liquid film-thicknesses (as shown in Figures 1.3 and 1.4) to the order of magnitude of the size of bubbles. As a result, the effective liquid-vapor phase that is at saturation temperature come very close, a distance Δ_F ($\ll$ film thickness Δ), to the higher wall temperatures on the boiling-surface i.e., saturation temperatures are just above the effective thermal boundary layer thickness Δ_F , as shown in the inset of Figure 1.4. This depicted equivalence (with Δ_F replacing the actual liquid film thickness Δ in Figure 1.3) is only for heat transfer rate improvements, the actual liquid flow mobility remains as in Figure 1.3.

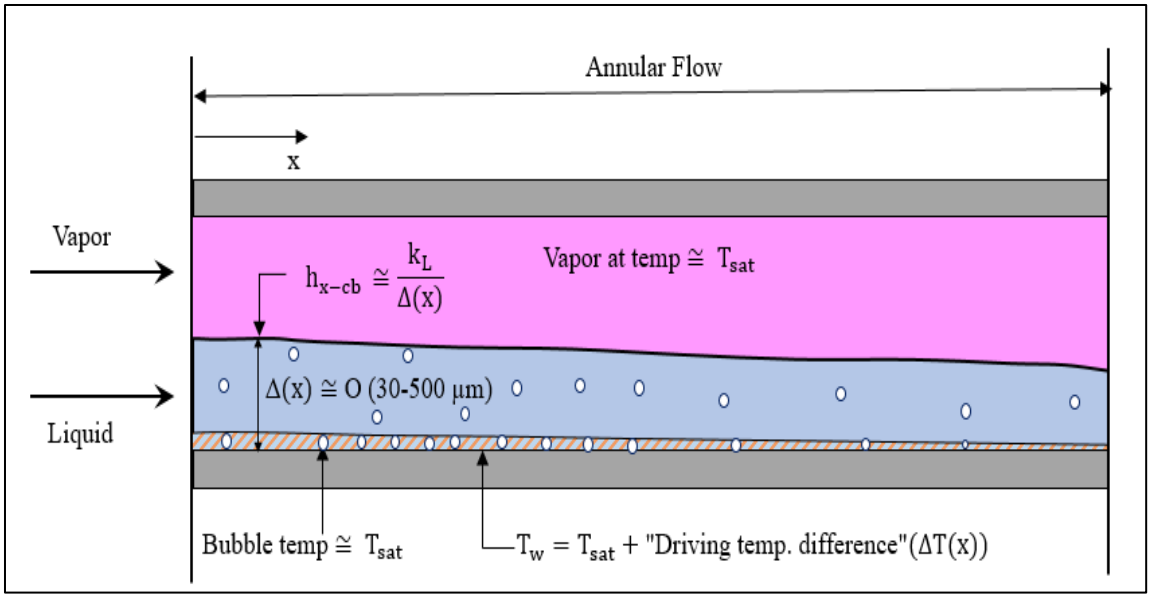

Figure 1.3. Presence of invisible μm- scale nucleation rates (bubble diameters less than 10 μm) for observed liquid thickness Δ ≅ O (100-300 μm) leads to an equivalent liquid thickness ΔF that is much less and is a result of micro-scale nucleation rates.

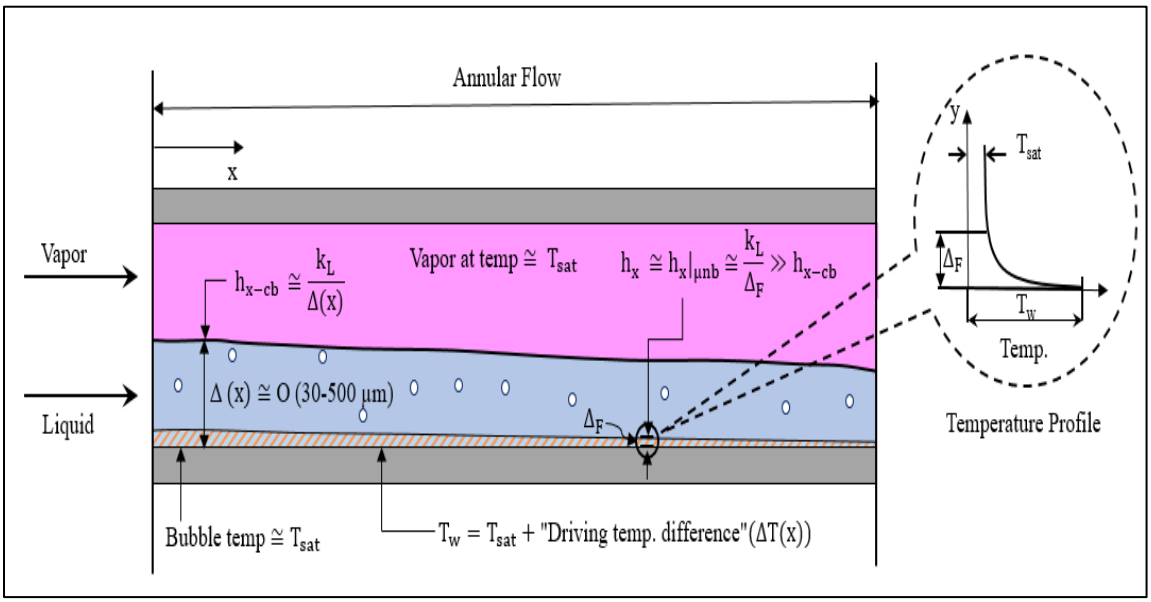

Figure 1.4. The figure shows enhanced HTC across equivalent liquid thickness ΔF. However, liquid flow mobility continues to be superior – as in Figure 1.3.

Since the above reported science results ([2-6]) require annular regime-B operations in Figure 1.2 – and they are technologically difficult to implement ([2], [13]) – the reported technological approach is based on a decision to operate in regime-A of Figure 1.1. This region is shown in Figure 1.5, where the new approach is best for inclusion of numerous micron-scale nucleating bubbles (depicted by small red circles in Figure 1.5).

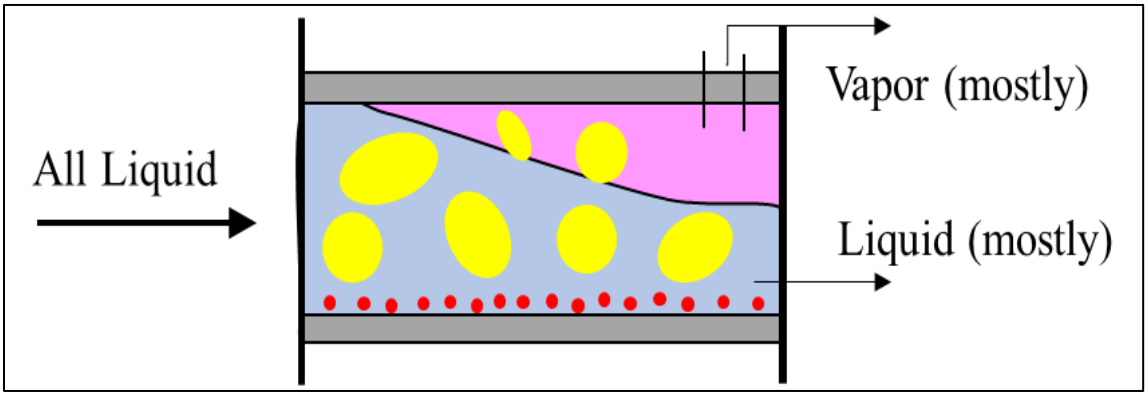

Figure 1.5. Nucleate/bubbly regime of operations with several new micron-sized bubbles (●) of diameter D_b induced by the proposed technology.

An implementable technology is however needed to create and sustain large scale micro-scale nucleation rates – which are indicated as red dots in Figure 1.5 above. Such a technology should provide for: (i) enhanced nucleation site-density at micron-scales – preferably by one of the inexpensive, effective, and passive micro-structuring – approaches [14]-[22]; (ii) suitable "in-plane" shear-mode minuscule vibrations, between any effective boiling-surface and its nucleating bubbles, to favorably impact the contact-line physics (see Figure 1.6) and associated time-scales (see Figure 1.7) that are known to be associated with nucleation mechanisms (see [7-12]); (iii) suitable "in plane" shear mode vibrations of the mesh-top tips to significantly alter the hydrodynamic forces on tiny nucleating and/or emerging bubbles that escape from the mesh-top (see Figure 1.9) so as to rip them off the

mesh-top at a smaller effective diameter (and, consequently, smaller thermal boundary-layer thickness Δ_F both in Figure 1.4 as well as in the preferred nucleate/bubbly regime of Figure 1.5) and larger frequency; and (iv) an adjustable control on the frequencies and amplitudes associated with the "in-plane" shear-mode minuscule vibrations (through a suitable controller, through a software/hardware arrangement, that is potentially upgradable by implementations of "machine learning" features) to achieve very significant energy efficiency via exploration of suitable resonance phenomena. The experimental approach used for achieving the above goals also has sufficient flexibility and cost-effectiveness, given the fact that although some of the nucleation mechanisms in pool/flow-boiling are qualitatively understood for larger diameter bubbles ([7]-[12]), they are not very well understood for micron-/nano- sized bubbles [23].

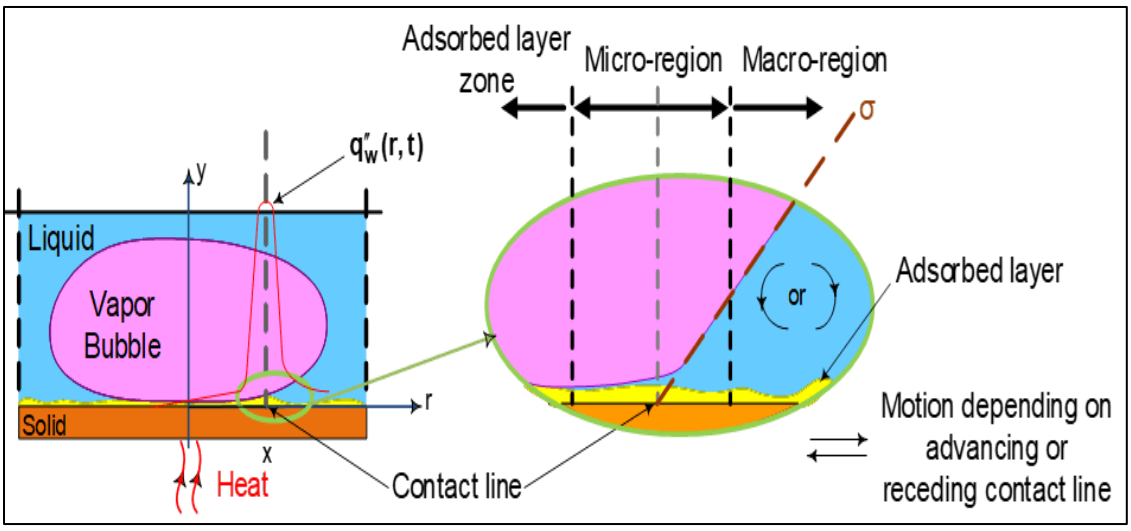

Figure 1.6. Mechanisms and contact-line physics for nucleate boiling ebullition cycle. The figure also highlights the significant heat-flux impact of advancing/receding dynamics of micro-layers and the role of oscillatory contact-line interfacial shear (whether induced entirely naturally by heat – or supplemented by mechanical actuation).

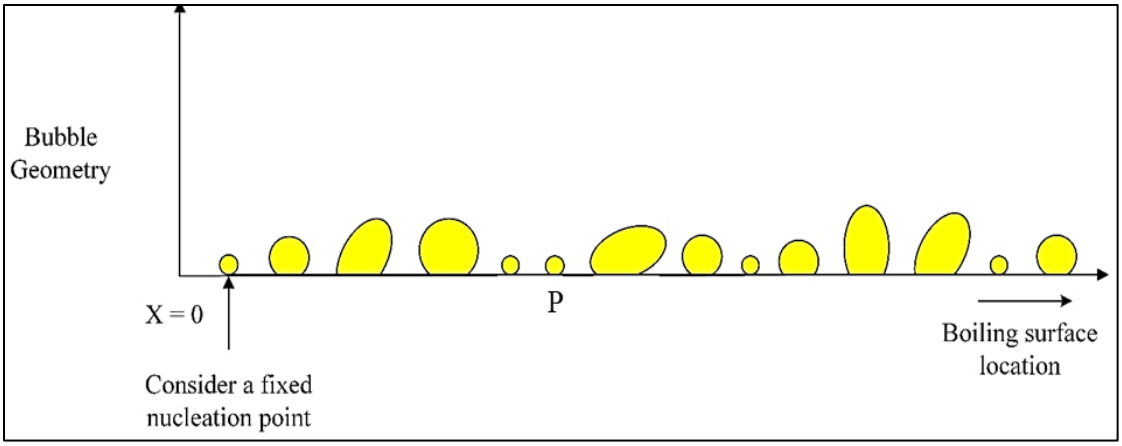

Figure 1.7. Bubble formation over the boiling surface at any instant time t.

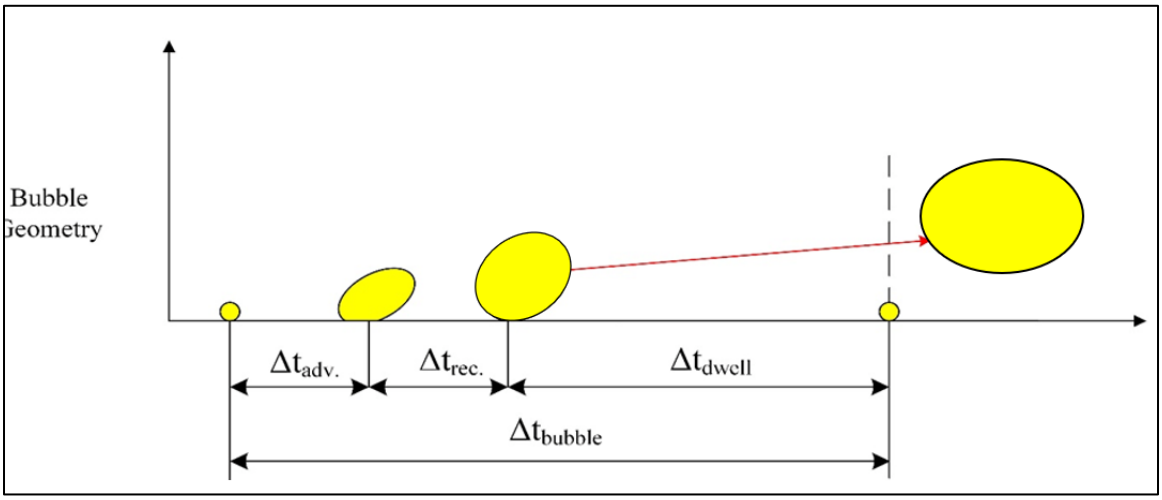

Figure 1.8. Time evolution of a bubble for a respective fixed location P – see (1.7) – on the boiling surface.

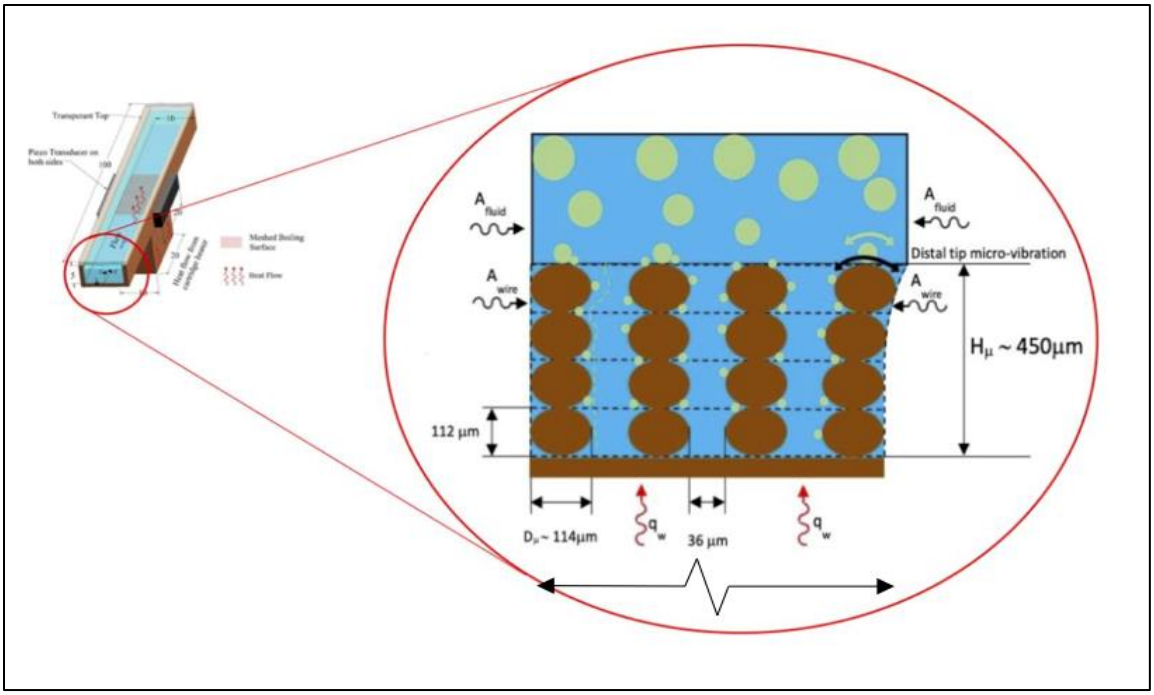

Figure 1.9. Cross-sectional view of a small portion of the boiling surface is taken from the test section in Figure 2.1, shows a mesh with piezo actuations. Only the last pillar (formed by stack of the copper mesh) in the above figure is shown displaced but all of them (entire mesh) vibrate at a resonant frequency. There are green nucleating vapor bubbles in the tiny crevices of the mesh which rise and are fed to a relatively larger bubble on the distal tip. The oscillating motion of the tip induce hydrodynamic forces that results in the dislodging of bubble at a much smaller diameter.

2 Experimental Setup and Description

The experiments involving flow boiling (as well as conditions representing pool boiling) of HFE–7100 use the test-section shown in Figure 2.1. The closed loop setup in Figures 2.2-2.4 deploys this test-section. The flow-loop also deploys an air cooled condenser, two peristatic pumps with embedded flowmeters, a reservoir, a copper tubing super heater, a pressure transducer, several thermocouples, and other accessories (such as valves, cartridge heaters, watt meters, Piezos' controller, etc.). Crucial data from this setup (acquired using a PC, NI DAQ and its accessories, LabVIEW software, etc.) are used for quantitative analysis of boiling heat transfer performance. The following paragraphs further explain the function of each part of the setup in a brief manner.

The flow channel (10 mm x 5 mm rectangular cross-section that is 100 mm long in the flow direction, see Figure 2.1) is cut, into a copper slab (which has other cuts) is called a copper tub – and is a part of the test-section (see Figures 2.2-2.4). The flow-channel's bottom-surface may – or may not, if it is a no-mesh experiment – have an approximate 0.45 – 0.5 mm thick meshed surface with microstructure. The meshed microstructure is obtained from diffusion bonding of four layers of a suitable copper-mesh (in this example: a square shaped 100 mesh, i.e. 100 copper wires, each of 114 μm diameter with 140 μm of spacing between a pair of wires, per 2.54 cm). Furthermore, the heated part of the test section's bottom-surface is only 10 mm x 20 mm in dimensions with the heating coming from imbedded electric heating cartridges (not shown in Figure 2.2 as the heaters lie below the cross-sectional areas) in an insulated heater block. Figures 2.2-2.4 show the temperature

measurements at locations 1, 2, 3, and 4 within the block (Figure 2.4), at location/temperature T_{bbp} associated with the bottom-surface of the boiling plate (Figures. 2.3-2.4) associated with the boiling-surface, and a location/temperature T_{mt-avg} for measurement of a *local* temperature on the top of the meshed boiling-surface. Average temperature/location T_{tbp} for the underside of the mesh and the top surface of the bottom boiler plate were not directly measured. An estimated or a representative value of this temperature T_{tbp} is, however, inferred from other temperature and heat flow rate measurements. Furthermore, the test-section channel has an in-built hole for liquid inlet (see Figure 2.4). There are two fluid exit ports, an in-built outlet (Figure 2.4) at the bottom in the horizontal copper-tub, which allows liquid and vapor mix of HFE–7100 to exit. There is a second arrangement for direct exit of HFE-7100's vapor phase. This is through a top-hole (see Figure 2.3) in the transparent polycarbonate cover of the copper tub. At steady heating, the net Joule heating of the insulated copper block is available, in W, from measurements obtained from Watt meters hooked up to the cartridge heaters along with time duration measurements. A photograph of the actual hardware associated with the experimental set up described in Figures 2.2-2.4 is shown in Figure 2.5.

Steady state experiments are run to obtain "heat-flux versus representative temperature-difference" curves for various liquid inlet flow rates. Inlet liquid mass flow rate values are kept above the lowest inlet liquid mass flow rate (a heat-flux dependent value) that corresponds to sufficient temperature-difference conditions (above ONB), at locations above the heated boiling-surface, allow pool-/flow- boiling dominated by nucleation rates. Here representative heat sink temperature-difference is taken to mean measured

temperature at location T_{bbp} (which govern boiling plate's top-surface temperature T_{tbp}, temperatures within the mesh, and two-phase thermal boundary-layer temperatures in the fluid above) minus the saturation temperature T_{sat} (see Figures 2.3 to 2.4) associated with the representative absolute pressure value (as estimated by the pressure transducer shown in Figures 2.1 to 2.4).

The "Heat Transfer Coefficient (HTC) versus representative heat-flux" curves are obtained for plain and meshed (micro-structured) boiling-surfaces - with and without cases involving suitable controller actuated excitations of the Piezos for generating acoustics-induced vibrations of the meshed region.

Transverse mode PZT-5A type Piezoelectric transducers were used. They were custom made (with suitable poling and dimensions of 20 mm x 4 mm x ~1.5 mm and resonant frequency of about 1 MHz – with values of about $460x10^{12}$ m/V or better – and dissipation factor "tanδ" value of about 0.017 or lower). The Curie temperatures of the Piezos used were 350^{o}C or higher. Piezos were placed as per the geometry depicted in Figure 2.1. The idea underlying their placement locations, as shown in Figure 2.1 and Figure 2.3, is to introduce uni-directional and bi-directional longitudinal acoustic waves' propagation in the copper base plate (A_{cu}), in the fluid (A_{fluid}), and in the mesh-wires (A_{wire}). The pair of Piezos, and their concurrent firing (although phase-lag options exist), ensured sufficient amount of acoustic energy in standing wave forms. The expected *differences in the amplitude and energy of waves* associated with A_{cu}, A_{fluid}, and A_{wire} are likely to introduce desired oscillatory in-plane shear stresses S_x and S_y (on top of the mesh) at locations where

nucleating bubbles are already experiencing contact line oscillations during the ebullition cycles (Figures 1.7 and 1.8) as well as strong hydrodynamic forces on the bubbles emerging from the mesh-top. Also, as discussed earlier, as shown in Figure 1.9, the idea is to cause mesh-tip structural vibrations to help in ripping-off the emerging nucleating bubbles, from the mesh-top, at a much smaller diameter (compared to cases without acoustic vibrations). Also, the high frequency of these bubbles' departure from the mesh-top and the dwell time replenishment of liquid there (Figure 1.8) and in the Wenzell filling micro-pores of the mesh (Figure 1.9), together create strong up and down convection currents within the mesh (which will help promote and transport sub-micron nucleate boiling in this region).

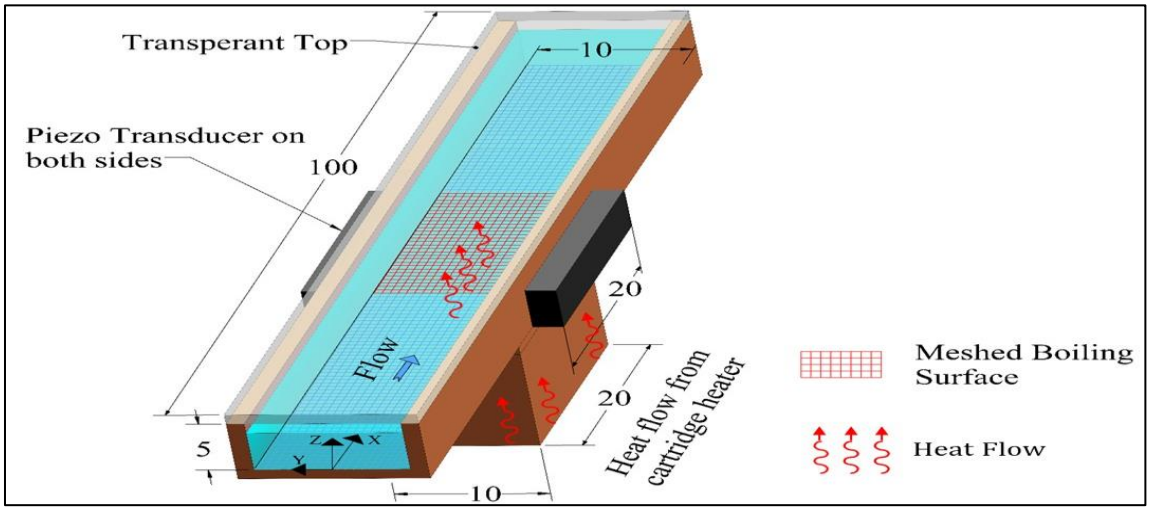

Figure 2.1. Test section

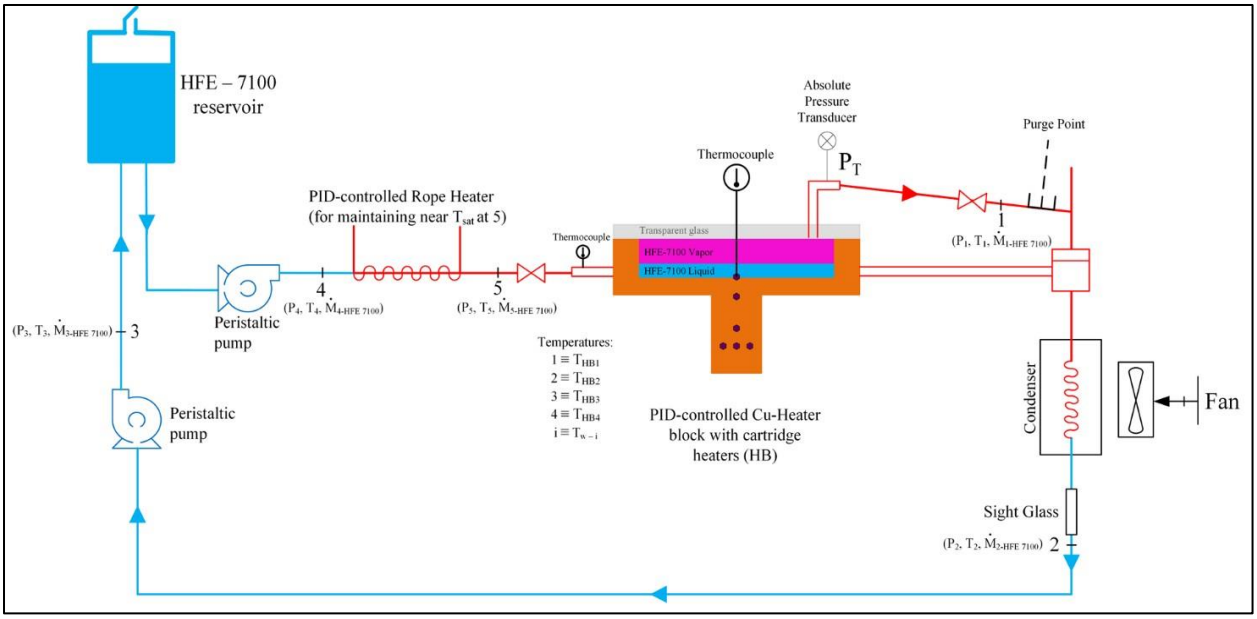

Figure 2.2. Standard arrangements of the experimental flow-loop.

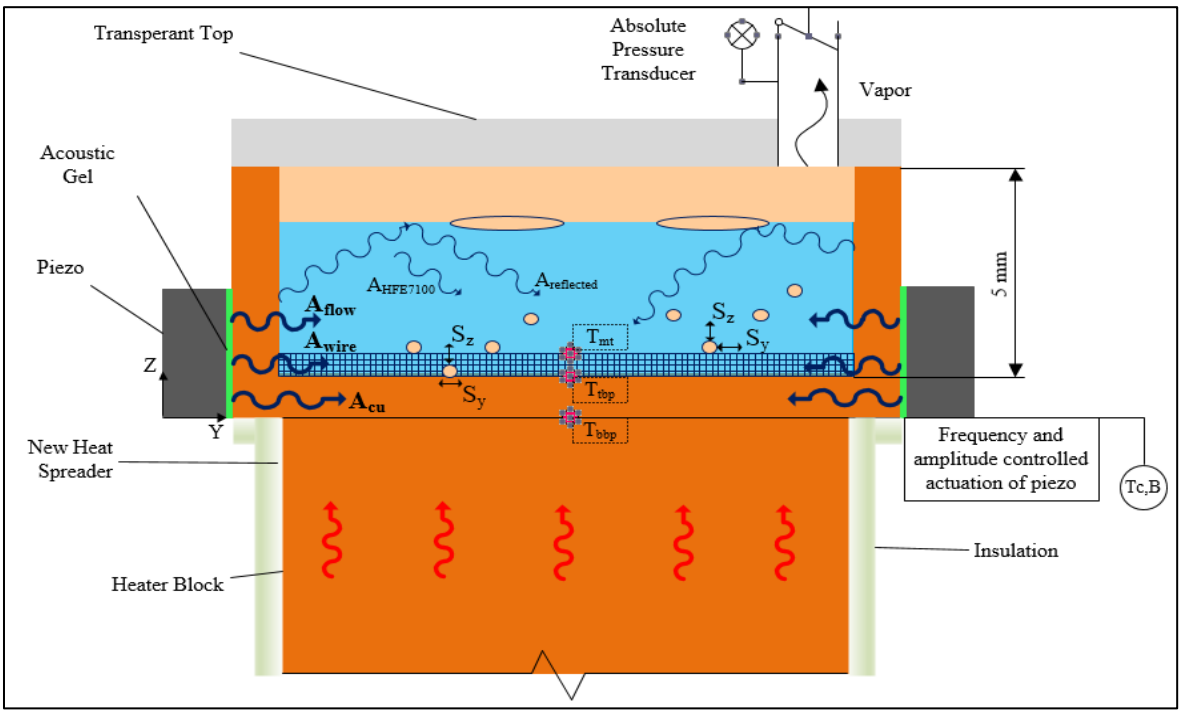

Figure 2.3. Axial cross-sectional view

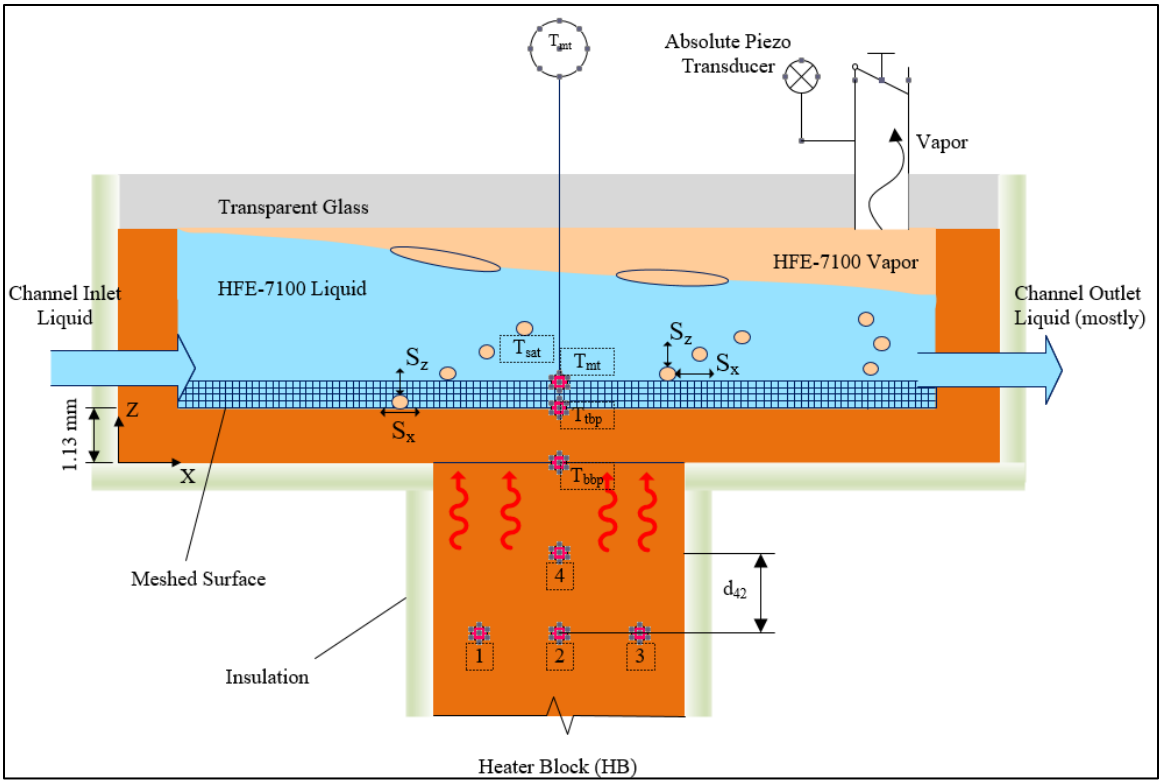

Figure 2.4. Lateral cross-sectional view

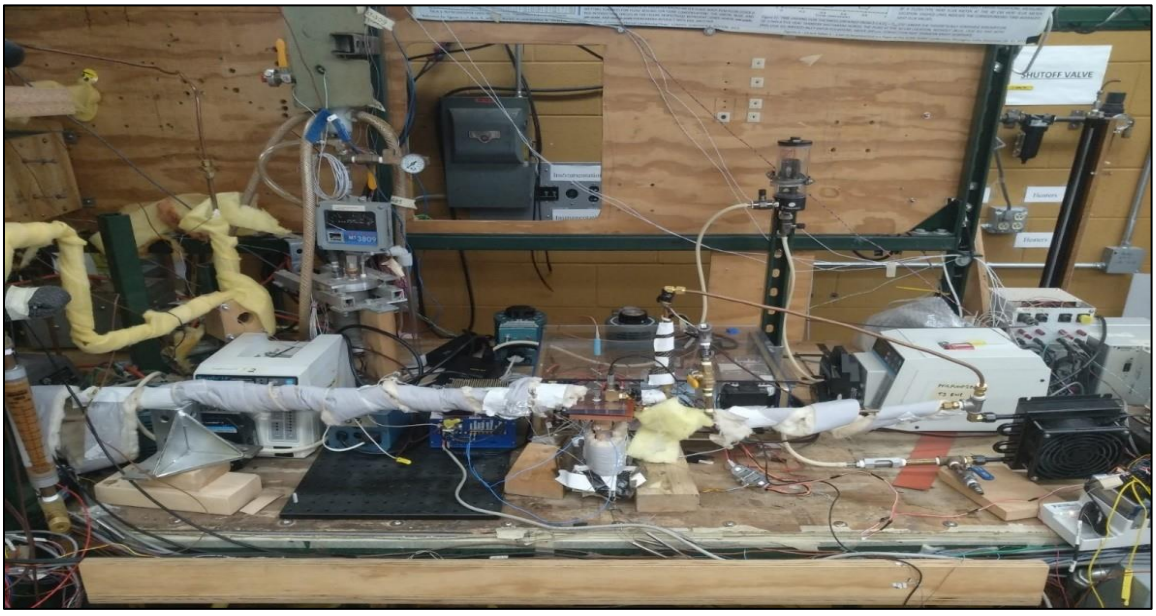

Figure 2.5. Experimental setup at present

3 Results

The entire set up – including the hardware and associated software – has been designed, manufactured, assembled and tested. Test runs were done for flow boiling (as well as close to "pool boiling") conditions. The flow-boiling regime was chosen to be a "nucleate/plug-slug regime" depicted in Figure 1.5– with inlet quality of zero (all liquid), and non-zero outlet quality (typically in the range of 0.19– 0.76).

In Figures 1.5 and 2.2-2.4, the flow-arrangements and controls allowed for leaving of a small vapor gap between the boiling-liquid and the top horizontal-surface of the channel, especially near the exit. For some runs, a stratified bubbly liquid flow topped by a vapor gap from inlet to exit was allowed, because the approach allowed for stronger arrival of acoustic waves at the horizontal boiling-surface's nucleation sites by way of reflections of the acoustic waves from the liquid-vapor interface at the top (as in Figure 2.3). This way the significance of top to bottom acoustic waves on nucleating bubbles was ascertained. However, it resulted in miniscule (1-5%) HTC enhancement in our experiments, as it did in earlier pool-boiling experiments of [24], relative to the more significant enhancements reported here where excitations were kept, predominantly, in the horizontal plane. Separate experiments (not reported here) were also performed where the acoustic waves were predominantly upward – from the bottom of the boiler plate to the top; these also yielded miniscule (1-5%) HTC enhancement. So, it was concluded that only an air gap near the exit would be necessary, as is the case with the more convenient bubbly and partial boiling

flow-regime of our experiments (excitations arrangement shown in Figure 1.5 and Figure 2.1).

For the experiments described in Section-2, data from several independent test-runs were obtained, and results analyzed for each of the test-runs. For cases involving non actuated Piezos and plane copper channel (i.e. without meshed bottom-surface), results from some flow-boiling runs were obtained for $\dot{M}_{L-in} > q''_w * A_{bs}/h_{fg}$, where h_{fg} is heat of vaporization - in J/kg - at a representative test-section pressure. The average heat-flux $\bar{q}''_w$ (W/cm^2) over the boiling-surface (of area A_{bs} = 2 cm^2) was estimated from total cartridge power measurements and the assumption of good insulation all around the heater block. It was also estimated for order of magnitude formula: $\bar{q}''_w \cong k_{cu} \cdot (\bar{T}_{HB2} - T_{HB4})/d_{42}$. These results were found to be in order of magnitude agreement with the value obtained from dividing the sum total of cartridge heater power supplied to the heater block (as obtained by sum total of Watt-meters' readings divided by the time duration of steady runs) by the boiling-surface area A_{bs}. The first estimate would actually overestimate the real values – given that heat leaks from the side surfaces of the heater block (which has less than perfect insulations). The second estimate $\bar{q}''_w \cong k_{cu} \cdot (\bar{T}_{HB2} - T_{HB4})/d_{42}$ will give lower values, because of 2-D heat flows in between the thermocouples and T_{bbp} measurement, reason being the presence of air gap in between them (see Figure 3.1). This air gap was placed for vertical excitation experiments (not described here) but is being removed from future experiments. Despite this, a more accurate heat-flux $\bar{q}''_w$ estimate (as well as other variables of interest here) than the first estimate is possible, and are being obtained with the help of

all the data and use of a full 3-D ANSYS/Fluent analysis as developed and described in [6]. These new results are only expected to improve, slightly, the errors and error estimates reported here in Figure 3.1.

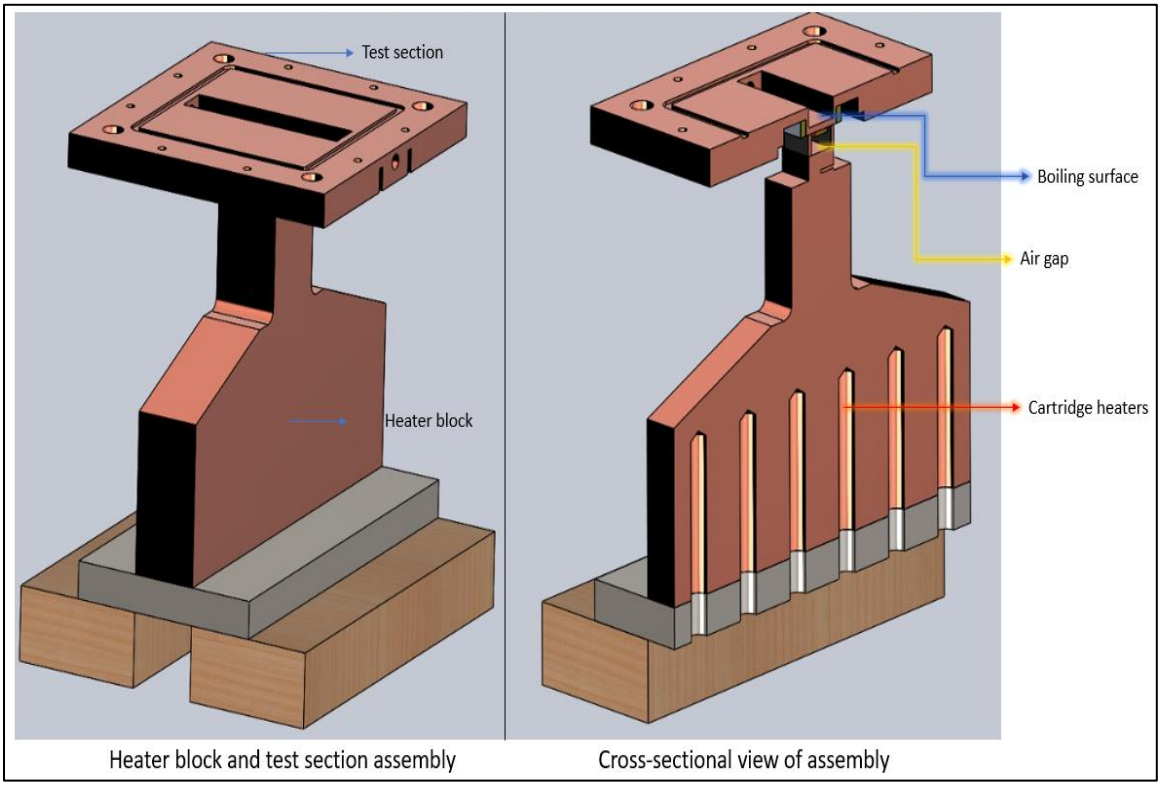

Figure 3.1. Heater block and test section assembly.

Table 1. Results from test runs for representative no-piezo actuation and plain copper boiling cases. The representative constant density of the liquid phase is denoted by ρ_L.

Test run	Approx. $\dot{M}_{L\text{-}in}/\rho_L$	$T_{mt-local}$	T_{bbp}	$P_{test-sec}$	T_{sat}	$\bar{T}_{HB2}$	ΔT_{rep}	$\bar{q}''_w$	HTC ($\bar{h}_{eff}$)	Quality (X_{exit})
	(mL/min)	(°C)	(°C)	(kPa)	(°C)	(°C)	(°C)	(W/cm^2)	(W/cm^2 - °C)	
	± 2 %	± 1%	± 0.1	± 3%	± 1%	± 1°C	± 1.1%	± 10%	± 11.04%	± 6%
1	40	58.4	120.79	102.5	61.81	58.4	58.98	40.8	0.6917	0.76
2	40	57.8	107.29	101.2	61.42	57.8	45.87	28.8	0.6278	0.54

For no-Piezo actuation case and use of meshed boiling-surface at the bottom surface of the heated copper channel exposed to fluid flow, results obtained from some flow-boiling runs (i.e. $\dot{M}_{L-in} > \bar{q}''_w * {A_{bs}}/{h_{fg}}$, where h_{fg} is heat of vaporization - in J/kg - at test-section pressure) are given in Table 2 below.

Table 2. Results from test runs for representative no-piezo actuation and meshed boiling surface cases. The representative constant density of the liquid phase is denoted by ρ_L.

Test run	Approx. $\dot{M}_{L\text{-}in}/\rho_L$	$T_{mt-local}$	T_{bbp}	$P_{test-sec}$	T_{sat}	$\bar{T}_{HB2}$	ΔT_{rep}	$\bar{q}''_w$	HTC ($\bar{h}_{eff}$)	Quality (X_{exit})
	(mL/min)	(°C)	(°C)	(kPa)	(°C)	(°C)	(°C)	(W/cm^2)	(W/cm^2 - °C)	
	± 2 %	± 1%	± 0.1	± 3%	± 1%	± 1°C	± 1.1%	± 10%	± 11.04%	± 6%
1	40	60	83	104.4	62.41	175	20.59	30	1.457	0.56
2	40	59.5	77.9	103.5	62.11	157.7	15.79	21.6	1.3679	0.4
3	40	59.5	72.4	102	61.66	121.9	10.74	12	1.1173	0.22

Figure 3.4 below plots $\bar{q}''_w$ versus HTC $\bar{h}_{eff}$ values for various cases of interest. In Figure 3.4, the 3 dark blue points at the bottom are for the "NO_MESH_EXPT" data and correspond to the plane copper boiling-surface results in Table 1 above. The 3 data points (second set from the bottom in green) for "WITH_MESH_EXPT" are the experimental values for flow boiling over meshed copper surface and they come from Table 2. Since ΔT_{rep} values dropped for micro-structured mesh use at a given heat-flux, the boiling efficiency measure HTC, $\bar{h}_{eff} \equiv \frac{\bar{q}''_w}{\Delta T_{rep}}$, is higher with respect to plane copper (no-mesh). The results imply, as is known [25], significantly improved boiling-efficiency. The

increasing % improvement in the HTC values (for the passive mesh-based micro structuring approach relative to plane copper) in Figure 3.4– with increasing heat-flux values – over the ranges of 10 – 40 W/cm^2 looks very promising for future experiments and development of capabilities for even higher heat-flux operating conditions. These micro structuring-based improvements, discussed later on, are known to occur due to increases in nucleation site density and decreases in the minimum superheat ΔT_{rep} (also denoted as $\Delta T_{rep|ONB}$) needed for *onset of micro-nucleate boiling* (ONB).

In Figure 3.4, near 30 W/cm^2, the "MESH+PIEZO_EXPT_1" data points in yellow (the next higher data set located above "WITH_MESH_EXPT" data) correspond to experimental runs for meshed boiling-surfaces with active piezo actuation given in Table 3 and "MESH+PIEZO_EXPT_2" a single data point in light green (topmost point in Figure 3.4) correspond to result in Table 4. Not only the actuation frequencies and amplitudes used for "MESH+PIEZO_EXPT_1" and "MESH+PIEZO_EXPT_2" are different for the two cases – in fact, for the topmost data point, even the meshed channel and the associated copper block hardware are different (but otherwise identical except, perhaps, in residual stress and strain in the mesh). So, the reported additional enhancements results, due to Piezos' actuation, are rather robust and promising for further explorations.

Table 3. Results from flow-boiling test runs for representative "meshed boiling-surfaces with piezos' actuation." The representative constant density of the liquid phase is denoted by ρ_L. The controller settings are given in the second column from the left. Number of pulses denote $\Delta t_{on} \cdot f_p$ values.

Test run	Approx. $\dot{M}_{L-in}/\rho_L$ (mL/min) ± 0.1	V_{DC}, Duty Cycle, f_{RF}, [V, #, MHz, #, Hz]	$T_{mt-local}$ (°C) ± 1	T_{bbp} (°C) ± 0.1	$P_{test-sec}$ (kPa) 3	T_{sat} (°C) ± 1 %	$\bar{T}_{HB2}$ (°C) ± 1°C	ΔT_{rep} (° C) ± 1.1	$\bar{q}''_w$ (W/cm^2) ± 10%	Quality X_{exit} ± 6%
1	40	[100, 0.5, 1.00, 1190, 420]	60.84	85.01	118.9	66.45	184	18.56	30	0.56
2	40	[100, 0.7, 1.00, 1750, 400]	60.33	85	126.28	68.39	184	16.61	30	0.56

Table 4. Results from flow-boiling test runs for representative "meshed boiling-surfaces with piezos' actuation." The representative constant density of the liquid phase is denoted by ρ_L. Totally different controller settings are associated with totally different hardware (copper block and meshed surfaces).

Test run	Approx. $\dot{M}_{L-in}/\rho_L$ (mL/min) ± 0.1	V_{DC}, Duty Cycle, f_{RF}, [V, #, MHz, #, Hz]	$T_{mt-local}$ (°C) ± 1	T_{bbp} (°C) ± 0.1	$P_{test-sec}$ (kPa) 3	T_{sat} (°C) ± 1 %	$\bar{T}_{HB2}$ (°C) ± 1°C	ΔT_{rep} (° C) ± 1.1	$\bar{q}''_w$ (W/cm^2) ± 10%	Quality X_{exit} ± 6%
1	40	[100, 0.5, 1.02, 500000, 1] Piezo ON & OFF for 1 second in rotation mode	60.4	63.99	130	69.2931	156.7	5.3	30	0.56

The two different cases for "meshed boiling-surfaces with piezos' actuation" at a heat-flux of about 30 W/cm^2, indicate an effective decrease in ΔT_{rep} of about 25 % and 55% with respect to the no piezo actuation case. Although the performance can be further improved with additional research, even these preliminary gains are quite repeatable and quite impressive because the decrease in $\Delta T_{rep} \equiv T_{bbp} - T_{sat}(P_{test-sec})$ with respect to no-Piezos cases is not due to decrease in T_{bbp}. In fact, T_{bbp} changes/increases just a little when Piezos are switched on. The decrease in $\Delta T_{rep} \equiv T_{bbp} - T_{sat}(P_{test-sec})$ is due to a significant and rapid increase in steady pressure $P_{test-sec}$ when Piezos are turned on and this leads to a significant increase in $T_{sat}(P_{test-sec})$. These observations – with regard to what

happens when Piezos are turned "on" or "off" – are more clearly illustrated by "ΔT_{rep}" and "$P_{test-sec}$" versus time "t" curves shown in Figure 3.8 below. The rapid increase in steady pressure $P_{test-sec}$ is due to steady "closed loop" operations in Figure 2.2 – with increased exiting vapor flow rates and decreased exiting liquid flow rates from the test-section, and yet a constant steady inlet liquid mass flow rate and a constant total exit mass flow rate downstream of the condenser. As a result of these flow-loop settings, the increased formation rates of bubbles in the test-section (as hypothesized earlier by red dots in Figure 1.5) lead to increased test-section pressures.

Average HTC $\bar{h}_{eff}$ which is determined by the experimental value of ΔT_{rep}, and it represents the three different experimental scenarios given in Tables 1 to 4. A thermal circuit modelling approach was used to separate out the flow boiling heat transfer coefficient ($\bar{h}_x$) component from the effective HTC ($\bar{h}_{eff}$) for the different experimental flow boiling scenarios, and based on this, a set of curves are plotted and presented in Figures 3.5 and 3.7.

The thermal resistances schematic in Figure 3.3 represents the thermal circuit where $R_{boiling}$ is the thermal resistance due to boiling, above the mesh-top or within the mesh, which changes as the HTC changes for different experimental configuration results mentioned above in relationship to the data reported in Figure 3.4. The thermal resistance R_{mesh} has both the resistances caused by thermal conductance through mesh and boiling within mesh. The thermal resistance $R_{boiling\ plate}$ is the resistance for the copper boiling plate. The

saturation temperature is denoted T_{sat}, the average mesh-top temperature is $T_{mt\text{-}avg}$, and the average top and bottom boiling plate temperatures are denoted T_{tbp} & T_{bbp}, respectively.

The thermal resistance equation for flow boiling over plain copper surface is given by:

$$\frac{1}{\bar{h}_{eff}.A_{bs}} = \frac{L_{bp}}{k_{bp}.A_{bs}} + \frac{1}{\bar{h}_{x}.A_{bs}} \tag{3.1}$$

which yields a modeled flow-boiling HTC (including nucleation rate contributions $\bar{h}_x \cong \bar{h}_{boiling-model}$) as:

$$\frac{1}{\bar{h}_{boiling-modeled}.A_{bs}} = \frac{1}{\bar{h}_{x}.A_{bs}} = \frac{1}{\bar{h}_{eff}.A_{bs}} - \frac{L_{bp}}{k_{bp}.A_{bs}} \tag{3.2}$$

From equation 3.2, value of $\bar{h}_x$ which is the HTC for "flow boiling on plain copper surface" is calculated based on the experimentally estimated values of HTC $\bar{h}_{eff}$. This is for the experimental setup of flow boiling over plain copper surface, with associated data given in Table 1. The thickness of the copper boiling plate is L_{bp} - which is the distance between locations/temperatures T_{bbp} and T_{tbp} – and its thermal conductivity is k_{bp}, and the one dimensionally heated boiling plate area is A_{bs}. The reason for introducing the additional nomenclature $\bar{h}_x \cong \bar{h}_{boiling-model}$ will be clearer from the thermal circuit discussions for "with mesh flow boiling" scenarios discussed next.

The thermal resistance equation for flow boiling over meshed copper surface is given by:

$$\frac{1}{\bar{h}_{eff}.A_{bs}} = \frac{L_{bp}}{k_{bp}.A_{bs}} + \frac{1}{A_{bs}.\bar{h}_{mesh}} + \frac{1}{A_{bs}.\bar{h}_{x}} \tag{3.3}$$

where, by incorporating any HTC contributions resulting from "within mesh" nucleate/flow-boiling in the $\frac{1}{A_{bs}.\bar{h}_x}$ term, we choose to write $\frac{1}{A_{bs}.\bar{h}_{mesh}}$ which has both the thermal conductance through mesh and boiling within mesh, and rewrite Eq. (3.3) as:

$$\frac{1}{A_{bs}.\bar{h}_{mesh}} + \frac{1}{A_{bs}.\bar{h}_x} = \frac{1}{\bar{h}_{eff}.A_{bs}} - \frac{L_{bp}}{k_{bp}.A_{bs}} \tag{3.4}$$

In equation (3.4), $\bar{h}_{eff}$ is the effective HTC for "flow boiling with mesh" given in Table 2. As the mesh is a porous media and nucleation likely takes place within the mesh as well, it is, in fact not an actual 1-D heat flow situation within the mesh – as adequately "modeled" here (for the purposes of quantifying enhancement, though not physics, and this is discussed in greater detail in the discussions section). Hence, the resistances due to conduction through the mesh, and boiling within mesh are coupled together and represented as a single modeled resistance as:

$$\frac{1}{\bar{h}_{boiling-model}.A_{bs}} = \frac{1}{A_{bs}.\bar{h}_{mesh}} + \frac{1}{A_{bs}.\bar{h}_x} \tag{3.5}$$

Similarly, with the above understanding of terms, the thermal circuit for "flow boiling over and within meshed surface - with piezo actuation" remains the same, and continues to be given by:

$$\frac{1}{\bar{h}_{eff}.A_{bs}} = \frac{L_{bp}}{k_{bp}.A_{bs}} + \frac{1}{A_{bs}.\bar{h}_{mesh}} + \frac{1}{A_{bs}.\bar{h}_x} \tag{3.6}$$

In the equation 3.6 $\bar{h}_{eff}$ is the effective HTC, calculated by dividing the measured/estimated value of $\bar{q}''_w$ by ΔT_{rep}, for "flow boiling over meshed surface with piezo actuation" given

in Tables 3 & 4. Here $\bar{h}_x$ is the actual HTC for the same scenario and $\bar{h}_{boiling-model}$ in the above equation remains the same as equation (3.5) with the understanding that $\bar{h}_x$ now includes the effects of Piezo actuation.

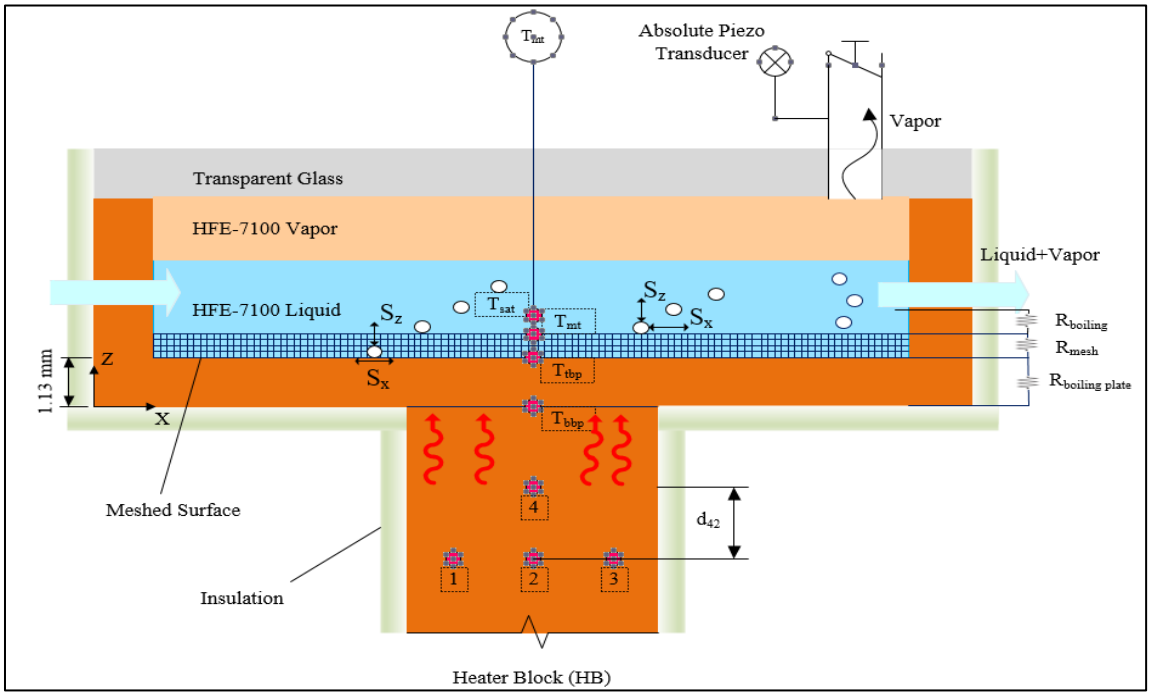

Figure 3.2. Resistance to the heat flux where $R_{boiling}$ represents the resistance in different conditions of boiling (no mesh, with mesh and mesh + piezo enhanced boiling). The effective resistance offered by the mesh is R_{mesh} and $R_{boiling\ plate}$ is the resistance due to the copper boiling plate below the mesh.

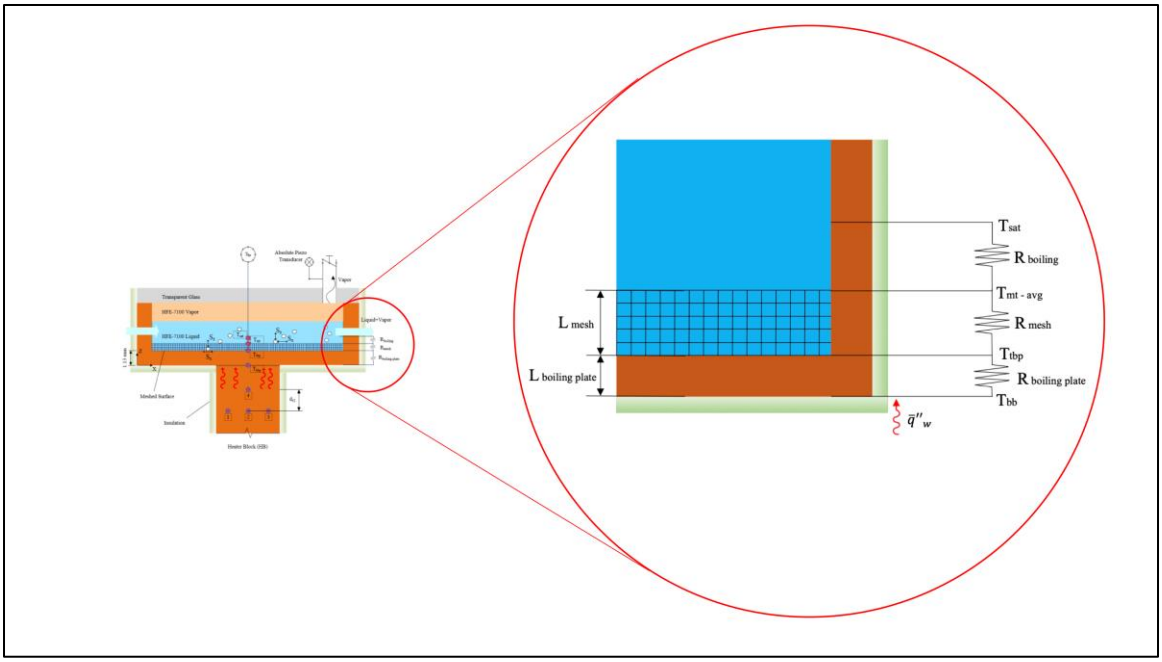

Figure 3.3. Thermal circuit.

The HTC component $\bar{h}_{boiling-model}$ is calculated based on the above equations and the experimental data obtained for different scenarios and is represented in Figure 3.1. The main question is how to augment (for trends) and connect the limited experimental data in Tables 1-4 and depicted as "points" in Figure 3-4 to predict guidelines for future, beyond Proof of Concept, experiments. The goal, for this purpose, is served by several correlations, available in the literature, which combine experimental data for different plain-surface flow-boiling scenarios that can yield HTC estimates and trends – provided their predictions are suitably corrected to fit a more specific (than what were used in the correlations) set of experimental data considered here. One such correlation is the Kim and Mudawar correlation [26] that determines the local (and allows estimates of the average $\bar{h}_{eff}$) heat transfer coefficient for plain-surface flow boiling. This correlation's data bank includes data from fluids, channel dimensions, and flow-regimes similar to the plain-surface flow

boiling experiments here. This correlation yields local HTC by calculating it through correlations for its two parts - which are termed nucleate and convective parts, whose names may be misleading [4-6] but that is irrelevant to the correlation for h_x and provides an estimate of the total heat transfer coefficient. This Kim and Mudawar Correlation [26] original, and its proposed corrected values $\alpha \cdot h_x$, are given through:

$$h_x = \left(h_{x|nb}^2 + h_{x|cb}^2\right)^{0.5} \tag{3.7}$$

where,

$$h_{x|nb} \equiv \left[2345\left(Bl\frac{P_H}{P_F}\right)^{0.7} P_R^{0.38}(1-X)^{-0.51}\right]\left(0.023\,Re_L^{0.8}Pr_L^{0.4}\frac{k_L}{D_h}\right) \tag{3.8}$$

And

$$h_{x|cb} \equiv \left[5.2\left(Bl\frac{P_H}{P_F}\right)^{0.08} + 3.5\left(\frac{1}{\tilde{X}_{tt}}\right)^{0.94}\left(\frac{\rho_V}{\rho_L}\right)^{0.25}\right]\left(0.023Re_L^{0.8}Pr_L^{0.4}\frac{k_L}{D_h}\right) \tag{3.9}$$

The parameters in the above definitions of h_x are:

$$Bl \equiv \frac{\bar{q}''_w}{G.\,h_{fg}}, \qquad P_R = \frac{p_o}{p_{cr}}, \qquad Re_L \equiv \frac{G(1-X)D_h}{\mu_L},\ Pr_L \equiv \frac{\mu_L C_{p,L}}{k_L}, \tag{3.10}$$

$$We_{L0} \equiv \frac{G^2 D_h}{\rho_L \sigma},\ \tilde{X}_{tt} = \left(\frac{\mu_L}{\mu_V}\right)^{0.1}\left(\frac{1-X}{X}\right)^{0.9}\left(\frac{\rho_V}{\rho_L}\right)^{0.5} \tag{3.11}$$

The main reason for using the above is our agreement with the correlation's total HTC h_x value in Eq. (3.7) with regard to its order of magnitude and trends – not the physics-based meanings (see [4-6]) of its convective and nucleate parts. The original Kim and Mudawar correlation [26] is for flow boiling over plain copper surface condition. This correlation, as it exists, is plotted for a range of heat flux values from 10 to 40 W/cm^2 for a mass flow rate of 40ml/min and is shown by the bottom most curve "KIM_MUDAWAR (K-M)" in Figure 3.4. This correlation is corrected by multiplying it by a factor α_{corr} = 3.92 to match with the $\bar{h}_{modeled}$ data which are calculated by the thermal circuit and experimental data for flow boiling over plain copper surface given in Table 1. The corrected HTC value is given by the second from the bottom curve "K-M_NO_MESH_CORRECTED".

It is then hypothesized that, over the heat-flux ranges in Figure 3.4, the modeling of observed enhancements in $\bar{h}_{eff}$ values in Figure 3.4 can be accomplished by a factor $\alpha = \beta \cdot \alpha_{corr}$ where the parameter $\beta > 1$ adequately captures the enhancement effects of flow-boiling on meshed-surface of a certain non-dimensional thicknesses and pore sizes with respect to the original channel height, as well as superposed effects of Piezos enhanced nucleation rates. With this understanding, α = 9.04 (and $\beta \cong 2.3$) for flow boiling over meshed copper surface without piezo actuation, with the resulting curve in Figure 3.4 labeled as "K-M_WITH_MESH_CORRECTED." Similarly α = 11.43 ($\beta \cong 2.91$) and 40.78 ($\beta \cong 3.92$) for the flow boiling over meshed surface with piezo actuations of two different types, with their effects shown by "K-M_MESH+PIEZO_CORRECTED_1" and "K-M_MESH+PIEZO_CORRECTED_2," respectively, in Figure 3.4.

The experiments were actually done at two different flow rates – 40 ml/min (as shown in Figure 3.4) and at 50 ml/min (not shown in Figure 3.4) – and the resulting 50 ml/min curve was only slightly above the curve in Figure 3.4. The proximity of the two curves for two different inlet liquid flowrates indicated significant limits of enhancement based on increasing the inlet liquid mass flow rates $\dot{M}_{L\text{-}in}$ and then seeing improved HTC values due to increasing bubble nucleation rates with the help of potentially increased hydrodynamic forces capable of dislodging more micron-sized nucleating bubbles. Therefore, the insignificant effects of increasing $\dot{M}_{L\text{-}in}$ is not studied here and the focus is on charactering the effects of increasing nucleation rates through "mesh" and "mesh plus Piezo" approaches.

Also, to gain an insight on the trends and HTC ($\bar{h}_{eff}$ and $\bar{h}_{boiling-model}$) values for future higher heat-flux experiments, these curves have been extended to get HTC values in Figures 3.6 and 3.7 (for heat flux ranging from 10-75 W/cm^2 and mass flow rate of 40ml/min, 82 ml/min and 112ml/min) to provide a tentative guideline for future experiments.

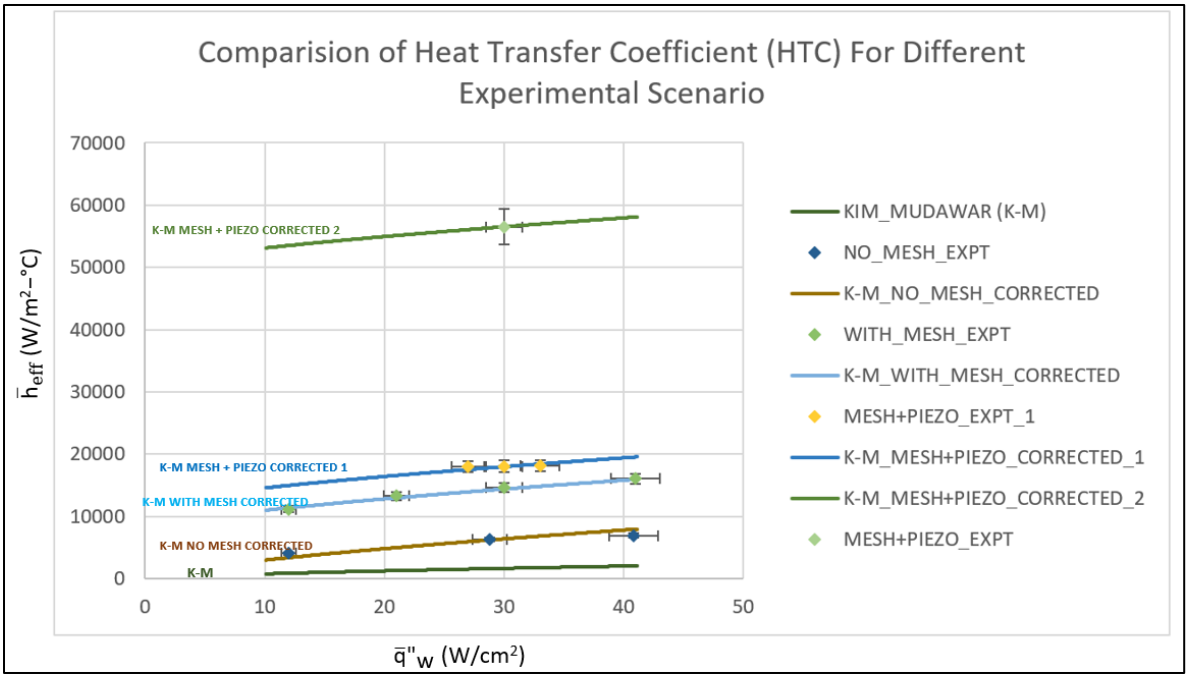

Figure 3.4. Heat Transfer Coefficient ($\bar{h}_{eff}$) vs Heat Flux Experimental data and Corrected K-M plots for three different experimental scenarios.

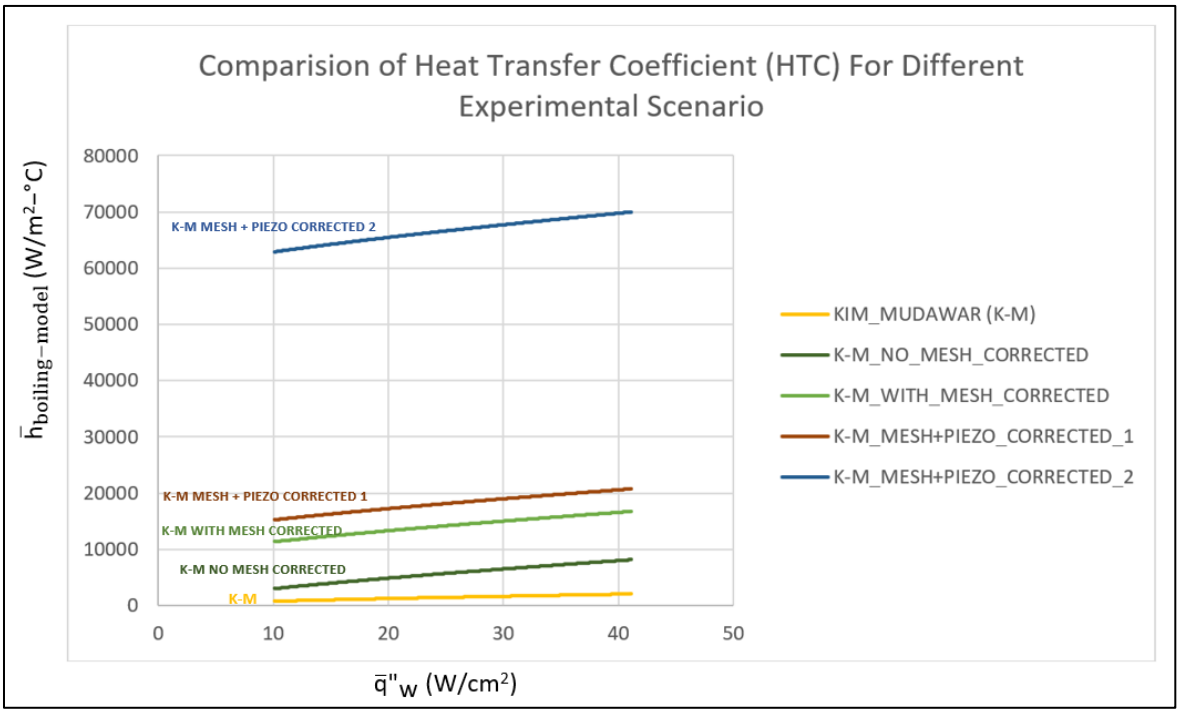

Figure 3.5. Heat Transfer Coefficient ($\bar{h}_{boiling-model}$) vs Heat Flux Corrected K-M plots for three different experimental scenarios

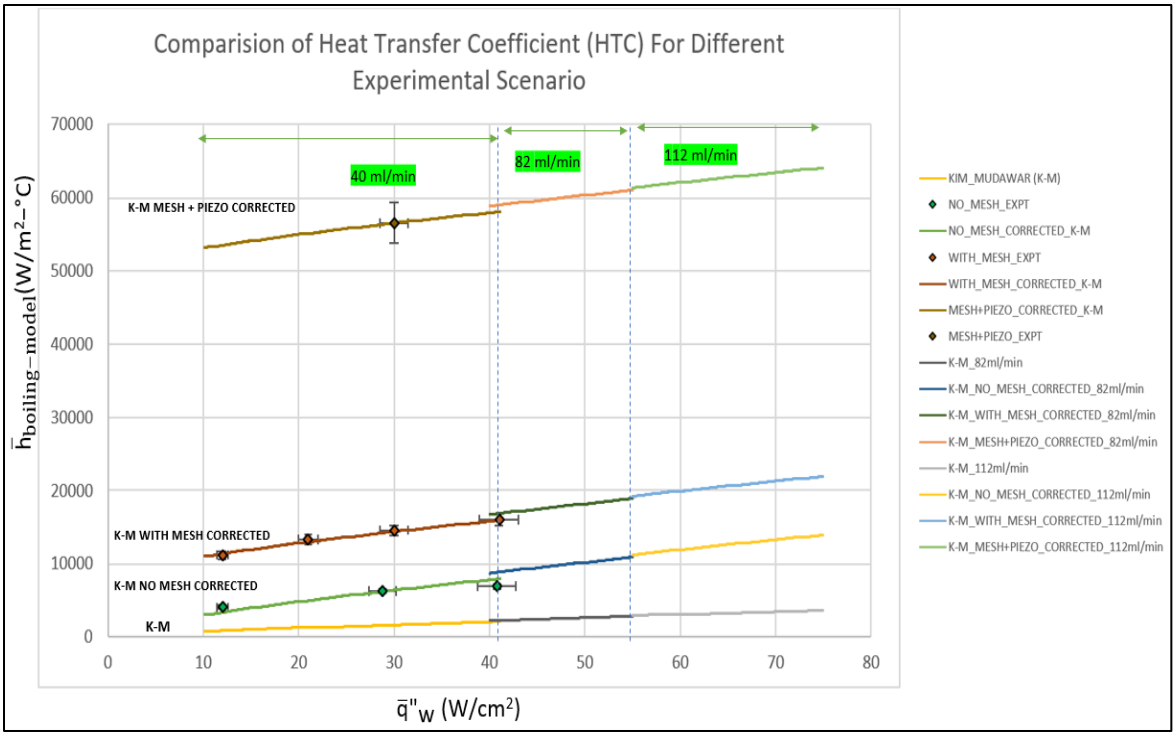

Figure 3.6. Heat Transfer Coefficient ($\bar{h}_{eff}$) vs Heat Flux Corrected K-M Blueprint.

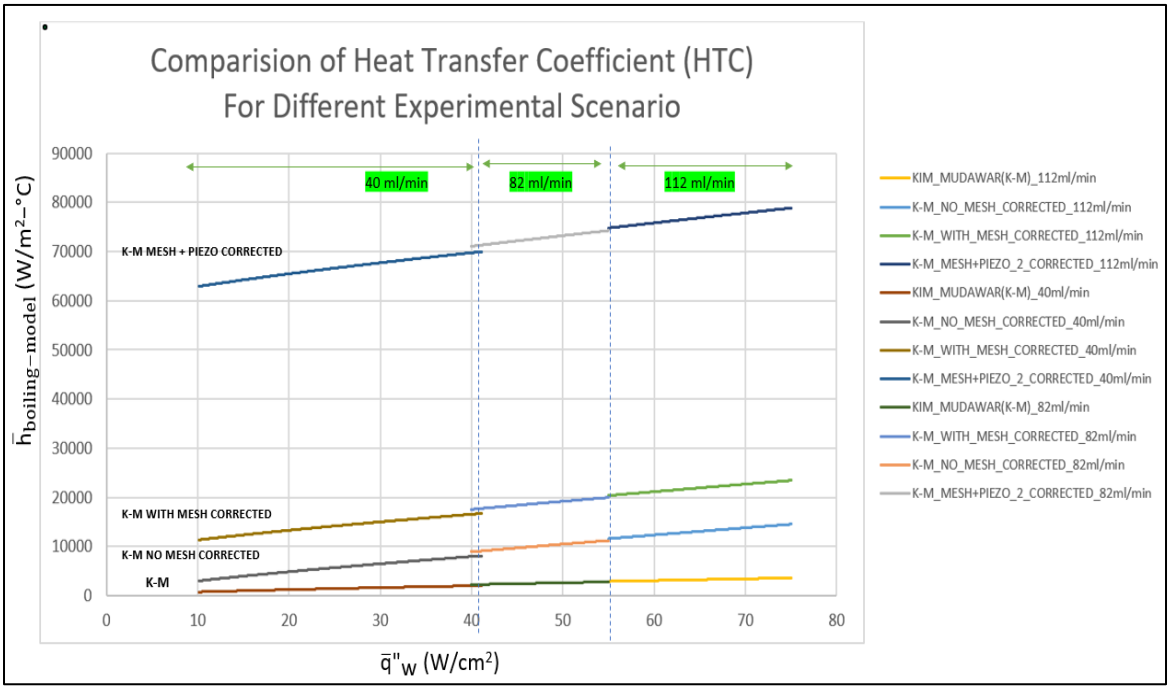

Figure 3.7. Heat Transfer Coefficient ($\bar{h}_{boiling-model}$) vs Heat Flux Corrected K-M Blueprint.

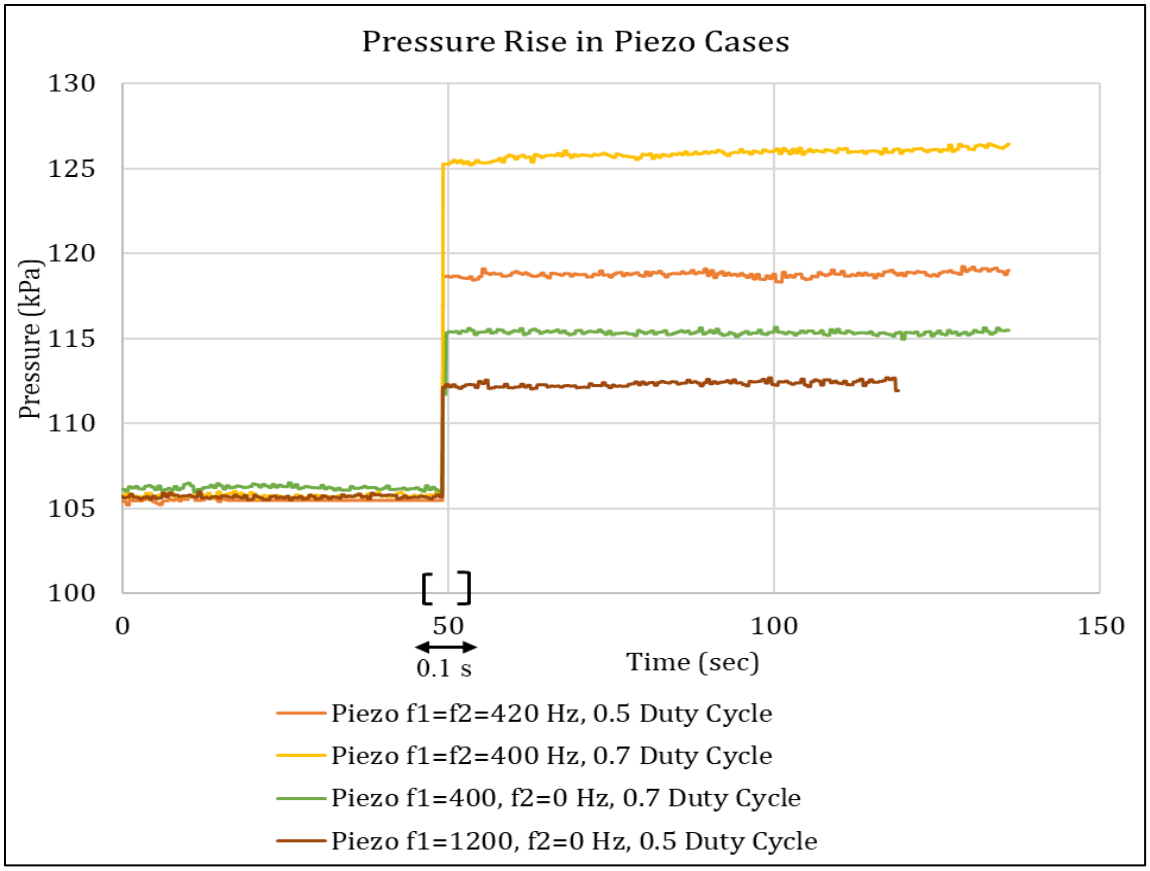

Figure 3.8. The test-section pressure's ($P_{test-sec}$) time response to increased micro-nucleation rates.

The test-section pressure's ($P_{test\text{-}sec}$) time response to increased micro-nucleation rates activated by Piezos' actuation at $t \cong 50$ s is shown. For $t \geq 50$ s, there are four different activations corresponding to four different controller settings described in the legend (with f1 and f2 respectively denoting the left and right Piezos' modulation frequencies f_M – and at the same duty cycle – as per definitions in Figure 2.1). For $t < 50$ s, the four "no-Piezos" steady flow-boiling realizations on meshed surface were roughly the same and corresponded to conditions characterized by: $\dot{M}_{L\text{-}in}/\rho_L \cong 40$ mL/min (approx.), $T_{bbp} \cong 84.64$ °C, $(P_{test-sec}) \cong 105$ kPa, $T_{sat}\,(P_{test-sec}) \cong 62.7$ °C, $\Delta T_{rep} \cong 21.9$ °C, $q''_w \cong 30$ W/cm^2 (approx.), and quality $X_{exit} \cong 0.56$.

4 Discussions

4.1 Micro Nucleating Bubble Diameter

The effective decrease in the two-phase thermal boundary layer thickness due to micro nucleation was responsible for enhancement in HTC in the annular flow boiling experimental results reported in [2-6] and depicted here in the inset of Figure 1.4. In the experimental approach described in this report for the flow-regime in Figure 1.5, the two-phase thermal boundary layer thickness (Δ_F) has a similar role and it is further reduced by using the new active approach of acoustic excitations, which enhance the micronucleation rates by favorably changing the hydrodynamic forces needed for shortening the time durations and sizes associated with the bubbles' ebullition cycles (see Figure 1.9). The acoustic vibrations imposed on the distal tip of the mesh, likely cause it to vibrate at low amplitude that dislodge nucleating or emerging bubbles at very small diameter (D_b^*) and larger frequencies than what they would be in the absence of Piezos' actuation. Their larger number density is due to an increase in site density caused by the mesh. The above flow-physics descriptions are supported by high HTC results in Figure 3.4, along with pressure rise peaks in Figure 3.8.

Piezo-electric accoustic excitations in Figure 3.8, in resonance with the natural in-plane micro-vibrations of the distal-tips of the mesh and the natural frequencies associated with the bubble ebullition cycles, provide for the necessary hydrodynamic forces and significant increase in associated nucleation site densities $n''_{av}(D_b^*)$ as well as associated bubbling frequencies $f_e(D_b^*)$. for the bubbles that finally emerge from the mesh-top. The averaged

$n''_{av}(D^*_b)$ and $f_e(D^*_b)$ values arise from, see [4], the spectral density functions for $n''(D_b)$ and frequency $f(D_b)$ – which means "$n''(D_b) * dD_b$" represents the number of emerging bubbles per unit area of the mesh-top (of a given surface-structure) associated with bubble departure diameter in the range of "D_b" to "$D_b + dD_b$," with $f = f(D_b)$ representing the frequency associated with emerging bubble departure diameter D_b. These variables (n" and f) may also depend on the local driving temperature differences $\Delta T(x) \equiv T_{tbp}(x) - T_{sat}(P_{test-sec})$. The new approach enables a significant rate of increase, relative to no-mesh and no-acoustic excitation in Figure 1.9, in $n''_{av}(D^*_b)$, and $f_e(D^*_b)$ values with decreasing D^*_b. The above described increases with decreasing D^*_b is consistent with an asymptotic power-law modeling of the product $n''_{av}(D^*_b).f_e(D^*_b)$ as D^{*-n0}_b, for some positive exponent n0 such that it causes the micronucleation heat-flux $\left[n''_{av}(D^*_b) * f_e(D^*_b)\right]\left\{\left(\frac{\pi D^{*3}_b}{6}\right).\rho_v\right\}h_{fg}.\Delta_F(D^*_b)$ to increase. In Figure 1.4, it is a reasonable assumption that the thermal boundary layer thickness $\Delta_F(D^*_b)$ decreases with D^*_b and is $O(D^*_b)$. This is consistent with the asymptotic power-law modeling of the function $\Delta_F(D^*_b)$ as D^{*m0}_b, for some positive number m0 with $m0 \geq 1$. But these asymptotic models also have to be consistent with the macroscopic hypothesis proposed in Figure 1.4 – which states that the local micronucleation heat-flux $\left[n''_{av}(D^*_b) * f_e(D^*_b)\right]\left\{\left(\frac{\pi D^{*3}_b}{6}\right).\rho_v\right\}h_{fg}.\Delta_F(D^*_b)$ which is also, approximately, equal to $k_L.[\Delta T(x)/\Delta_F(x)]$ and increases with decreasing $\Delta_F(x)$. This implies a heat-flux increase rate at D^{*-m0}_b. Together with the asymptotic models, the equality of the two heat-flux models require: $D^{*-n0+m0+3}_b \sim D^{*-m0}_b$. This, in turn, implies n0-2m0 ≈ 3 and, therefore, n0 ≥ 5. Assuming n0 ≈ 5 for annular regime flow-boiling on plane

copper (see [4]), n0 ≈ 5.5 – 6 for flow-boiling on meshed copper, and n0 > 6.5-7 for Piezos enhanced flow-boiling for the flow-physics elucidated in Figure 1.9, one gets an inkling of different conditions that must be arranged, and improved upon, to arrive at the strong enhancement results reported here.

4.2 Thermal Circuit and Mesh Top Temperatures

The three different setups for experimentation are flow boiling on plain copper surface, flow boiling on meshed boiling surface and flow boiling on meshed boiling surface with piezoelectric transducer actuations. The future experimental plan is to take accurate average temperature readings of the copper mesh top T_{mt-avg} (the reported experiment only takes readings of a local temperature $T_{mt-local}$ for the mesh-top, and those readings are discussed below) via infrared thermometry to better understand the enhancement flow-physics and better quantify the heat transfer coefficient (HTC) modeling approach proposed here. The enhancement in each case has been quantified by calculating the $\bar{h}_{boiling-model}$ term that appears in the total thermal resistance model given through Eqs. (3.5) - (3.6). Future more accurate temperature readings, flow visualizations, and vibration characterizations (through 3-D laser vibrometry) of the mesh, at different depths of its layers, can be used to develop further physical insights into the underlying micro nucleation phenomena.

The proposed $\bar{h}_{boiling-model}$ component of HTC is for boiling over and within the meshed surface as well as over and within the piezo actuated meshed surface. This is because the mesh has porosity and nucleation likely takes place within those small cavities, as a result

there are even smaller sub-micron bubbles nucleating inside the mesh pores before they emerge and eject from the top of the mesh. Therefore, the effective total thermal resistance in Figure 3.3 has contributions from the boiler plate, the heat-transfer phenomena within the copper mesh (including time-averaged two-phase content within the fluid and conduction through its wires), dynamic bubble ejection and nucleation phenomena on the top of the copper-mesh, and two-phase fluid (HFE7100) flow above the mesh-top. The time-averaged ratio of fluid and vapor entrapped in the pores of a mesh can further depend on multiple causative parameters such as the surface-structure, contact angles at nucleation sites, wicking effect, vapor entrapment versus transport as determined by convection currents within the pores, etc.

Current experimental measurements reported in the Tables give some "local" mesh top temperature $T_{mt\text{-}local}$. They are found to be slightly below (by 1-2^{o}C) the saturation temperature of HFE7100. As the temperature sensor locally touches the top layer of the copper mesh, it predominantly measures the copper wire temperature of the top mesh layer. The fact that there is boiling occurring inside the pores, may allow a sideways transfer of heat at the porous mesh-top layers for growth of nucleating bubbles within. If this is true on the average, it may imply that most of the heat is transferred for growth of small intermittent bubbles inside the pores, which are then fed by internal convection currents to the bubbles that intermittently emerge and eject at the top of mesh, as shown in Figure 1.9. This sideways transfer of heat from the copper wires in the interior to the intermittent and sub-micron nucleating bubbles would increase interior convection HTC that the wires are exposed to and may significantly decrease the total thermal resistance to the path of vertical

heat conduction flow through the copper mesh (as compared to purely conductive resistance of the mesh in the absence of interior boiling).

4.3 Contact Angle

The knowledge about the spreading of fluid on a plane-surface and the very important role it plays in nucleate boiling is relatively well understood. In such experiments, HFE-7100 is a hydrophilic liquid whose static contact angle is $< 1^0$. The dynamic contact angle for pool boiling is known to be equal to 46^0 [27] which can take a different value during flow boiling or boiling under strong convection currents in the pores of the mesh. The role of dynamic contact angle can only be assessed via experimentation. The prediction of dynamic contact angle, which we believe is also influenced by the piezo actuation, and its control by the hydrodynamic forces is not our goal and can be considered to be one of the many goals of independent future experiments.

The wetting of micro-structured surfaces under isothermal conditions are broadly classified by the two extremes of Wenzel filling and Cassie-Baxter type interior dryness [28]. Here, for the chosen mesh, HFE-7100, isothermally floods the pores of a meshed surface (a Wenzel filling, as indicated in Figure 4.1) and it requires heating from below to provide the necessary higher superheat for the onset of nucleate boiling. For the chosen dimensions of mesh the HFE-7100, during static conditions, Wenzel filling, as shown in Figure 4.1, was experimentally observed. This is a necessary step towards ensuring that there are no large pockets of air left deep into the porous layers of mesh, which can reduce CHF value

and can cause an early appearance of instabilities that cause transition from nucleate to film boiling. However, the contact angle hysteresis during boiling is very different.

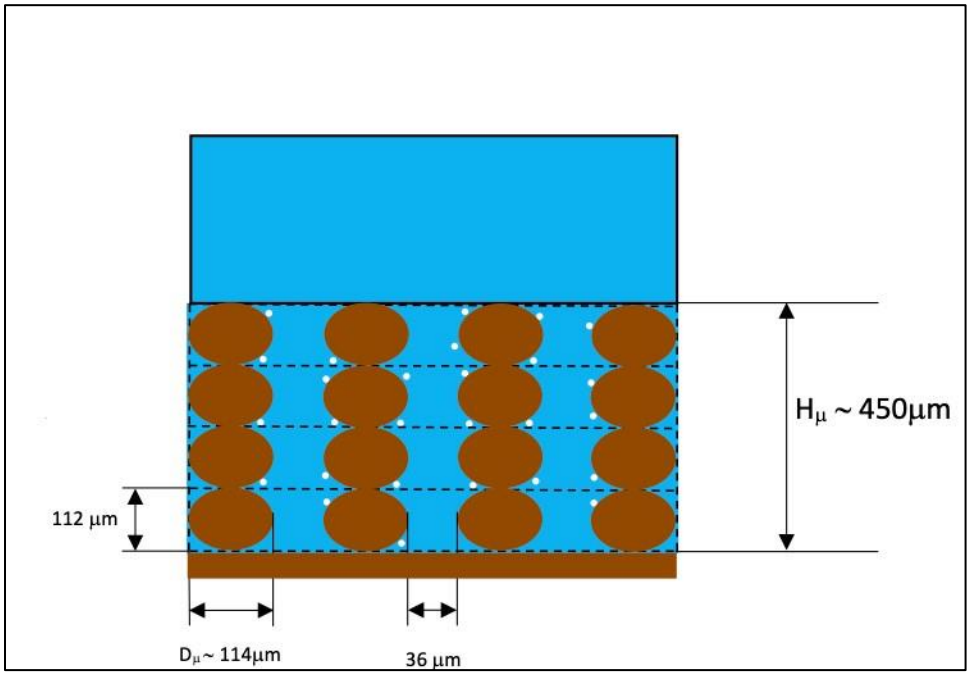

Figure 4.1. Wenzel filling of the mesh with tiny white spots as potential nucleation sites on the mesh.

4.4 Other Related Insights/Discussions of the Underlying Flow-Physics

The heat transfer of interest here is piezoelectric actuated, but controlled and enhanced, nucleation rates associated with heterogeneous boiling that takes place with growth and departure of vapor bubbles. These bubbles typically arise due to heat induced vaporization within trapped gases inside small cavities (typical nucleation sites) which are in contact with the boiling surface (mesh interior or mesh-top). The growth of a specific vapor bubble

and its detachment from a boiling surface location within the mesh, and formation of a new bubble after a dwell time is called the bubble's ebullition cycle. In case of within-mesh nucleating bubble's ebullition cycle, the cycle time is intimately connected to its motion within the fluid in the mesh pore and the bubble ebullition cycles of possibly larger bubbles that emerge at, and escape from, the mesh-top. These ebullition cycles act like numerous tiny engines, converting thermal energy received from the boiling-surface (s) to mechanical pumping energy resulting in bubbles' motions. These motions, in turn, lead to efficient heat-transfer from an *effective* boiling-surface, considered here to be the mesh-top. The heat transfer into the boiling fluid is facilitated by continual transport of higher enthalpy vapor bubbles rising from the effective boiling surface into the bulk liquid and ensuing transport of cooler saturated liquid rushing in to fill the empty space. This happens during a bubble's dwell time (see Figure 1.8), for a bubble that periodically depart from the mesh-top (without the presence of advance and recede time, if bubble is merely emerging and not nucleating at the mesh-top). The significant within-mesh temperature variations over the dwell time is also associated with transient conduction underneath the mesh-top as well as the fluid layer above it. Moreover, since the specific heat of the liquid is typically much smaller than the high latent heat of vaporization associated with nucleation rate phenomena, mostly interior to the mesh in the present situation, also play a very significant role – for all the well-known plane-surface boiling conditions (pool boiling, nucleate regime of flow-boiling, and even the so-called convective-regime ([2]-[6]) of flow-boiling) –- except for a very thin liquid film flows (often < 10 micro-meters) evaporative regimes.

Here additional HTC enhancements have been achieved during the boiling by increasing the rate of heat transfer via nucleating bubbles. Here it was done by a combination of passive and active approaches, as discussed in section 4.1.

The mesh surface can effectively increase the HTC but it can also result into an earlier attainment of critical heat flux if the pore sizes are so small that they do not promote Wenzell filling under isothermal conditions and, instead, promote Cassie-Baxter conditions.

The high wetting nature along with chosen values of pore-sizes result in Wenzel like [27] flooding of HFE-7100 into the meshed cavities on top of the boiling-surface. This apparent reduction in large number of nucleation site densities would have caused problems if all the vaporization was occurring at the mesh-top. In fact, for interior nucleation, imposed heating conditions lead to an actually larger number of nucleation site densities for imposed heat-fluxes and surface temperatures above ONB (onset of nucleate boiling) for the copper wires inside and around the pores' internal cavities formed at the high enough temperature junctions where the wires touch each other (see Figure. 1.1). Another important parameter introduced here is active and "tunable" micron-scale vibrations of the mesh wires and mesh-tips in Figure1.2. This is done by a controller that allows frequency/amplitude modulations of the natural resonant frequency of the piezoelectric transducer. These modulated frequency vibrations are in turn resonant with the structure and ebullition cycle frequencies and have a significant impact on determining the dominant sizes and frequencies that emerge from the mesh top. The double resonance features (one electrical

and one associated with structural and bubble frequencies) also significantly reduce the net energy consumption involved in the active actuation processes.

5 Future Scope and Directions

This work helps plan for new experiments dealing with piezoelectric transducer enhanced flow boiling over a meshed surface. This is being undertaken by an undergraduate senior design team under the guidance of Dr. Narain and his graduate research team.

6 Conclusions

Important insights were developed for future experimentations and existing Kim-Mudawar correlations were successfully corrected to match with the limited experimental data in order to predict the heat transfer coefficient and performance of future experiments - for a larger range of heat fluxes and inlet mass flow rate values.

7 Reference List

1. Narain, A., Vivek, V., Pandya, D., Sepahyar, S., 2019, "Nucleation control system and method leading to enhanced boiling based electronic cooling." Non-Provisional Patent Filed on November 12, 2019. Application No. PCT/US2019/060994.

2. Gorgitrattanagul, P. "Experimental investigations of temperature controlled innovative annular flow-boiling of FC-72 in millimeter scale ducts – steady and enhanced pulsatile realizations." Ph. D. Thesis, Michigan Technological University, December 2017. Two associated Journal Papers are being submitted.

3. Soroush Sepahyar, "Influence of Micro-nucleate Boiling on Annular Flow Regime Heat Transfer Coefficient Values and Flow Parameters - For High Heat-Flux Flow Boiling of Water." Ph. D. Thesis, Michigan Technological University, December 2017. One associated Journal Paper is being submitted.

4. Narain, A., H. Ranga Prasad, Gorgitrattanagul, P, S. Sepahyar and Mehendale, S, "Significant Role of Heat carrying Micro-scale Nucleation Rates for Steady Annular Flow boiling (Traditionally termed Convective Regime), Part I: Modeling/simulations support for assessments of experimental data." **To be submitted**.

5. Gorgitrattanagul, P., A. Narain, R. Kumar*, A. Ghate, and D. Pandya, "Significant Role of Heat carrying Micro-scale Nucleation Rates for Steady Annular Flow boiling (Traditionally termed Convective Regime), Part II: Experiments for Low Heat-flux Operations with FC-72 as a Working Fluid." **To be submitted**.

6. Soroush Sepahyar, Michael Kivisalu, Harsha Sathi, and Amitabh Narain, "Significant Role of Heat Carrying Micro-scale Nucleation Rates for Steady Annular Flow boiling (Traditionally termed Convective Regime), Part III: Experiments for High Heat-flux Operations with Water as a Working Fluid." **To be submitted**.
7. Kuo, Chih-Jung, Ali Kosar, Yoav Peles, Steven Virost, Chandan Mishra, and Michael K. Jensen. "Bubble dynamics during boiling in enhanced surface microchannels." *Journal of Microelectromechanical Systems* 15, no. 6 (2006): 1514-1527.

8. Mchale J P, Garimella SV (2010) Bubble nucleation characteristics in pool boiling of a wetting liquid on smooth and rough surfaces. International Journal of Multiphase Flow, 36 (4)**:** 249-260.

9. Kandlikar, Satish G. "Heat transfer mechanisms during flow boiling in microchannels." In *ASME 2003 1st International Conference on Microchannels and Minichannels*, pp. 33-46. American Society of Mechanical Engineers, 2003.

10. Bigham, Sajjad, and Saeed Moghaddam. "Microscale study of mechanisms of heat transfer during flow boiling in a microchannel." International Journal of Heat and Mass Transfer 88 (2015): 111-121.

11. Moghaddam, Saeed, and Ken Kiger. "Physical mechanisms of heat transfer during single bubble nucleate boiling of FC-72 under saturation conditions-I. Experimental investigation." International Journal of Heat and Mass Transfer 52, no. 5-6 (2009): 1284-1294.

12. Kunkelmann C, Ibrahem K, Schweizer N, Herbert S, Stephan P, Gambaryan-Roisman T (2012) The effect of three-phase contact line speed on local evaporative heat transfer: Experimental and numerical investigations. *International Journal of Heat and Mass Transfer*, 55 (7-8)**:** 1896-1904.

13. Kivisalu, M. T., Gorgitrattanagul, P., and Narain, A., "Results for High Heat-Flux Flow Realizations in Innovative Operations of Milli-Meter Scale Condensers and Boilers." *International Journal of Heat and Mass Transfer*. 2014, **75**, pp. 381-398.
14. Radek, Norbert, Łukasz J. Orman, Andrej Kapjor, and Augustín Sladek. "Efficient surfaces for boiling heat transfer enhancement." *Czasopismo Techniczne* 2016, no. Mechanika Zeszyt 4-M 2016 (2016): 3-8.

15. Chu, Kuang-Han, Ryan Enright, and Evelyn N. Wang. "Structured surfaces for enhanced pool boiling heat transfer." *Applied Physics Letters* 100, no. 24 (2012): 241603.

16. Chien, Liang-Han, and Ralph L. Webb. "A nucleate boiling model for structured enhanced surfaces." *International Journal of Heat and Mass Transfer* 41, no. 14 (1998): 2183-2195.

17. Li, Chen, Zuankai Wang, Pei-I. Wang, Yoav Peles, Nikhil Koratkar, and G. P. Peterson. "Nanostructured copper interfaces for enhanced boiling." *small* 4, no. 8 (2008): 1084-1088.

18. Chu, Kuang-Han, Young Soo Joung, Ryan Enright, Cullen R. Buie, and Evelyn N. Wang. "Hierarchically structured surfaces for boiling critical heat flux enhancement." *Applied Physics Letters* 102, no. 15 (2013): 151602.

19. Dong, Lining, Xiaojun Quan, and Ping Cheng. "An experimental investigation of enhanced pool boiling heat transfer from surfaces with micro/nano-structures." *International Journal of Heat and Mass Transfer* 71 (2014): 189-196.

20. Kuo, Chih-Jung, Ali Kosar, Yoav Peles, Steven Virost, Chandan Mishra, and Michael K. Jensen. "Bubble dynamics during boiling in enhanced surface microchannels." *Journal of Microelectromechanical Systems* 15, no. 6 (2006): 1514-1527.

21. Mchale JP, Garimella SV (2010) “Bubble nucleation characteristics in pool boiling of a wetting liquid on smooth and rough surfaces.”, *International Journal of Multiphase Flow*, 36 (4): 249-260.

22. Kandlikar, Satish G., and Chinmay Patil. "Enhanced Boiling with Selective Placement of Nucleation Sites." U.S. Patent Application 15/305,020, filed June 22, 2017. Also 2017/0176114

23. Agarwal, Ashutosh, Wun Jern Ng, and Yu Liu. "Principle and applications of microbubble and nanobubble technology for water treatment." *Chemosphere* 84, no. 9 (2011): 1175-1180.

24. Heffington, S., and A. Glezer. "Enhanced boiling heat transfer by submerged ultrasonic vibrations." In *Proceedings of the Therminic*. 2004.

25. Radek, Norbert, Łukasz J. Orman, Andrej Kapjor, and Augustín Sladek. "Efficient surfaces for boiling heat transfer enhancement." *Czasopismo Techniczne* 2016, no. Mechanika Zeszyt 4-M 2016 (2016): 3-8.

26. Kim, S. M., and Mudawar, I., 2013, “Universal approach to predicting saturated flow boiling heat transfer in mini/micro-channels – Part II. Two-phase heat transfer coefficient,” International Journal of Heat and Mass Transfer, **64**, pp. 1239-1256.

27. Thiagarajan, Suraj Joottu, Ronggui Yang, Charles King, and Sreekant Narumanchi. "Bubble dynamics and nucleate pool boiling heat transfer on microporous copper surfaces." International Journal of Heat and Mass Transfer 89 (2015): 1297-1315.

28. Banerjee, S. "Simple derivation of Young, Wenzel and Cassie-Baxter equations and its interpretations." *arXiv preprint arXiv:0808.1460* (2008).